Journal of Asian Earth Sciences 78 (2013) 301–317

Contents lists available at SciVerse ScienceDirect

Journal of Asian Earth Sciences

journal homepage: www.elsevier.com/locate/jseaes

Crustal density structure from 3D gravity modeling beneath Himalaya and Lhasa blocks, Tibet

Zhiming Bai [a,*], Sufang Zhang [a], Carla Braitenberg [b]

[a] State Key Laboratory of Lithospheric Evolution, Institute of Geology and Geophysics, Chinese Academy of Sciences, Beijing 100029, China
[b] Department of Geosciences, University of Trieste, Via Weiss, I-34127 Trieste, Italy

ARTICLE INFO

Article history:
Available online 10 January 2013

Keywords:
Density
Subduction angle
Lithological composition
Ecologitization
Himalaya
Lhasa
Tibetan plateau

ABSTRACT

The Himalaya and Lhasa blocks act as the main belt of convergence and collision between the Indian and Eurasian plates. Their crustal structures can be used to understand the dynamic process of continent–continent collision. Herein, we present a 3D crustal density model beneath these two tectonic blocks constrained by a review of all available active seismic and passive seismological results on the velocity structure of crust and lower lithosphere. From our final crustal density model, we infer that the present subduction-angle of the Indian plate is small, but presents some variations along the west–east extension of the orogenic belt: The dip angle of the Moho interface is about 8–9° in the eastern and western part of the orogenic belt, and about 16° in the central part. Integrating crustal P-wave velocity distribution from wide-angle seismic profiling, geothermal data and our crustal density model, we infer a crustal composition model, which is composed of an upper crust with granite–granodiorite and granite gneiss beneath the Lhasa block; biotite gneiss and phyllite beneath the Himalaya, a middle crust with granulite facies and possible pelitic gneisses, and a lower crust with gabbro–norite–troctolite and mafic granulite beneath the Lhasa block. Our density structure (<3.2 g/cm^3) and composition (no fitting to eclogite) in the lower crust do not be favor to the speculation of ecologitized lower crust beneath Himalaya and the southern of Lhasa block.

1. Introduction

With the advent of the theories of continental drift and plate tectonics, it has become widely accepted that the Tibet plateau is the product of the collision between the Indian subcontinent and the Eurasian continent and that this process of mountain building is still continuing today (Holmes, 1965; Dewey and Bird, 1970; Powell and Conaghan, 1973; Le Fort, 1975; Molnar et al., 1977; Xia et al., 2011; Wang et al., 2012). The Indian subcontinent is moving towards the Eurasian continent at a rate of 50 mm/yr (Minster and Jordan, 1978; Chatterjee et al., 2012) with respect to Eurasia plate. Owing to this ongoing tectonic evolution, the Tibet plateau has attracted the interest of geoscientists over many decades. Where, numerous geophysical studies have played an important role on understanding crustal evolution from the continent–continent collision recorded by the crustal structure. This crustal structure beneath the Tibetan Plateau started to be delineated with the series of Sino–French seismic studies (Hirn et al., 1984a,b, 1995; Min and Wu, 1987; Teng et al., 1985; Xiong et al., 1985; Galve et al., 2002; Zhang and Klemperer, 2005, 2010; Jiang et al., 2006), the Sino–American PASSCAL broadband experiment (McNamara et al., 1997; Owens and Zandt, 1997), the results of the international and multidisciplinary INDEPTH experiments (Zhao et al., 1993; Makovsky et al., 1996; Nelson et al., 1996; Zhao et al., 2001), and a large number of geophysical methods have been used to study the lithosphere of the Himalaya and Tibet regions, such as deep seismic investigations (Hauck et al., 1998; Galve et al., 2002; Haines et al., 2003; Meissner et al., 2004; Jiang et al., 2006; Zhang et al., 2009a,b, 2010, 2011a,b; Zhang and Klemperer, 2005, 2010; Chen et al., 2012; Hu et al., 2012), seismic tomography (McNamara et al., 1997; Villasenor et al., 2001; Chen et al., 2009a), magnetotellurics (Wei et al., 2001; Unsworth et al., 2004), gravimetry (Jin et al., 1996; Braitenberg et al., 2000, 2003; Shin et al., 2007), receiver functions (Kind et al., 1996) seismology (Mitra et al., 2005; Chen et al., 2009b, 2012; Zhang et al., 2011c) and geothermics (Chung et al., 2005).

It is well-known that the formation of the high Tibetan plateau from the Indian-Eurasia plate collision is strongly dependent upon each of the following parameters on the configuration of the elastic plate and on the gravity anomalies: the flexural rigidity, the position of the northern end of the elastic plate (the amount of underthrusting of such a plate beneath the Himalaya range), and the density contrasts between the crust and the mantle and between the sediments and the crust (Caen and Molnar, 1983).

* Corresponding author. Tel.: +86 10 82998345; fax: +86 10 82998229.
E-mail addresses: bbzzmmi@mail.iggcas.ac.cn (Z. Bai), berg@units.it (C. Braitenberg).

1367-9120/$ - see front matter © 2013 Elsevier Ltd. All rights reserved.
http://dx.doi.org/10.1016/j.jseaes.2012.12.035

In order to understand the flexural rigidity and density structure of the two elastic plates of the collision, many 2-D gravity models have been proposed recently. Rajesh and Mishra (2003) models the Bouguer anomaly along longitude 90°E for latitude 25–40°N across Himalaya and Tibet based on the results of INDEPTH seismic profiles across Tibet. In that work it is suggested that the crustal thickness varies from 40 km under the Indo-Gangetic Plains to 70 km under the Indus Tsangpo Suture Zone (ITSZ), remains almost constant at 70 km under the Tibet and reduces to 40 km north of Altyn Tagh Fault (ATF). The crustal vertical section is divided into three layers of bulk densities (2.7, 2.8 and 2.9 g/cm^3), with two low-density layers (2.65 and 2.69 g/cm^3) at the bottom of the upper and middle crusts respectively, which are layers with low seismic velocities. Hetenyi et al. (2007) combined seismological and Bouguer anomaly data with 2-D thermo-kinematic and petrological modeling to constrain the extent and kinetics of the eclogitization process in the Indian lower crust underthrusting Tibet. Based on Airy-type isostasy gravity modeling, they showed that the presence of denser material (eclogite) is required beneath the Lhasa block. Three profiles perpendicular to the Himalayan arc with multilayer density-models suggest that the process of eclogitization of the Indian lower crust is completed where the maximal depth of its descent is reached. The petrologic modeling results of Hetenyi et al. (2007) showed many similarities but also some differences in the three profiles. The similarities lie in the fact that, at the very first order, the geometry of the Moho is quite similar along each profile: it starts at 35 km of depth in the South and ends at about 75 km of depth beneath the Tibetan plateau. The major density variation of the Indian lower crust occurs once it reaches its maximum depth. The differences between the three profiles are also related to their geometries: the steepness and the localization of the lower crust's descent are particular to each profile. Between profile P1 and P2 (see detail in Hetenyi et al. (2007)), the differences are small: profile P2 shows a somewhat steeper dip, located closer to the front of the range compared to profile P1, but both profiles reach their maximum depth in one ramp. This is not the case for profile P3: there is a flat part in the descent of the lower crust between two ramps, and constraints on the geometry (even if they are less tight) suggest that it plunges at a lower angle and on a longer distance than profiles P1 and P2. Thus the gradual change of density also takes place on a larger distance. One additional difference is the geometry of the foreland basin: while data are well explained by a flexural form at profiles P1 and P2, it is better represented with a shallower, flat-bottom basin at profile P3, as previously mentioned by Tiwari et al. (2006). Jimenez-Munt et al. (2008) presented a 2-D lithospheric temperature structure and density model along a north–south transect from the Indian plate to Asia, crossing the Himalaya front and the Tibetan Plateau. The model is based on the assumption of local (Airy) isostatic equilibrium, and it is constrained by the topography, gravity and geoid anomalies and by thermal data within the crust. Their results suggest that the height of the Tibetan Plateau is compensated by thick crust in the south and by hot upper mantle to the north. The Tibetan Plateau as a whole cannot be supported isostatically only by thickened crust; a thin and hot lithosphere beneath the northern plateau is required to explain the high topography, gravity, geoid and crustal temperatures. The lithosphere reaches a maximum depth of ~260 km beneath the southern Plateau, and thins abruptly northward to ~100 km under the central and northern Plateau. The lithosphere depth increases again beneath the Qaidam basin and the Qilian Shan to ~160 km (Zhang et al., 2008; Jimenez-Munt et al., 2008).

With the use of potential field methods in Tibet and using terrestrial data, Braitenberg et al. (2000) proposed a map of 3-D undulations of the Moho and discussed the properties along four profiles cutting the Tibet plateau longitudinally and transversally. They applied an inversion-method of the gravity field throughout the entire plateau and later showed (Braitenberg et al., 2003) that there are considerable flexural rigidity variations when going from the Tibet plateau to the cratonic Tarim basin. Shin et al. (2007) presented a 3-D model of the Moho undulations over the entire Tibetan plateau derived from gravity inversion using the Gravity Recovery and Climate Experiment (GRACE) potential field, which has been integrated with terrestrial data. This Moho model is characterized by a sequence of troughs and ridges with a semi-regular pattern, which could reflect the continent–continent collision between the Indian and Eurasian plates.

There are still numerous problems to answer, such as a plate with a constant flexural rigidity of about 0.7×10^{25} Nm allows a good fit to the data from the Lesser Himalaya and the Ganga Basin (Caen and Molnar, 1983). However, such a plate cannot underthrust the entire Himalaya. Instead, the gravity anomalies show that the Moho steepens from an inclination of about only 3° beneath the Lesser Himalaya to about 15° beneath the Greater Himalaya (Caen and Molnar, 1983). This implies a smaller flexural rigidity beneath the Greater Himalaya than beneath the Ganga Basin and the Lesser Himalaya. They predict rapid uplift only in the Greater Himalaya and at the foot of the Lesser Himalaya. The interpretations of densely seismic and seismological observations (Zhang and Klemperer, 2005) addressed the west–east difference of the crustal structure between the eastern part of central-south Tibet and the western part, which should be reflected in potential dataset. In order to obtain 3D crustal density model beneath Himalaya and Lhasa blocks, we apply a 3-D gravity modeling with constrains of other geophysical observations.

As mentioned above, the structure of the Tibet is being investigated by different approaches and at different sites. The 2D gravity models have given promising results, which can be expanded by a full 3D modeling. Furthermore, the density structures of the published studies have low lateral and vertical resolution, which we intend to improve in our 3D study. We integrate seismic with the gravity modeling, in order to obtain an improved understanding of petrological properties from the rock densities and velocities. This will allow us to have a better understanding of the actual physical state of the crust in this continent–continent collisional area. Many high-resolution seismic studies in Tibet (Xiong et al., 1985; Xiong and Liu, 1997; Zhao et al., 2001; Liu et al., 2003; Li, 2003; Zhang et al., 2002; Zhang et al., 2005; Chen et al., 2009a,b) provide very good constraints on the geometry of crustal structure and the seismic wave velocity profiles which we use in our gravity modeling. In this study, Bouguer anomaly data are used to: (1) obtain the crustal density structure and to delineate the regional variations of the crustal structure in the subduction zone, (2) define the depth of the Moho and the flexure of the Indian shield, and (3) check the eclogitization of the Indian lower crust.

2. Brief description of gravity anomaly dataset

Fig. 1 shows the gravity data used in this study, which mainly are $10' \times 10'$ gridded Bouguer anomalies, and the same as used in Braitenberg et al. (2003). The grid data was based on the Chinese gravity network 85, with height reference of the Yellow Sea (Sun, 1989). The gravity data were reduced using the Helmert gravity formula (Sun, 1989). A complete terrain correction was made, with a maximum radius of 166.7 km and using a topographic density of 2.67 g/cm^3. In order to obtain data coverage over a rectangular grid, which necessarily goes beyond the Chinese border, the data were integrated with Bouguer gravity values derived from the IGG97L (Institute of Geodesy and Geophysics, CAS, Wuhan) earth gravity model (Hsu and Lu, 1995). The gridded data have been integrated outside the Chinese territory with gravity data derived from

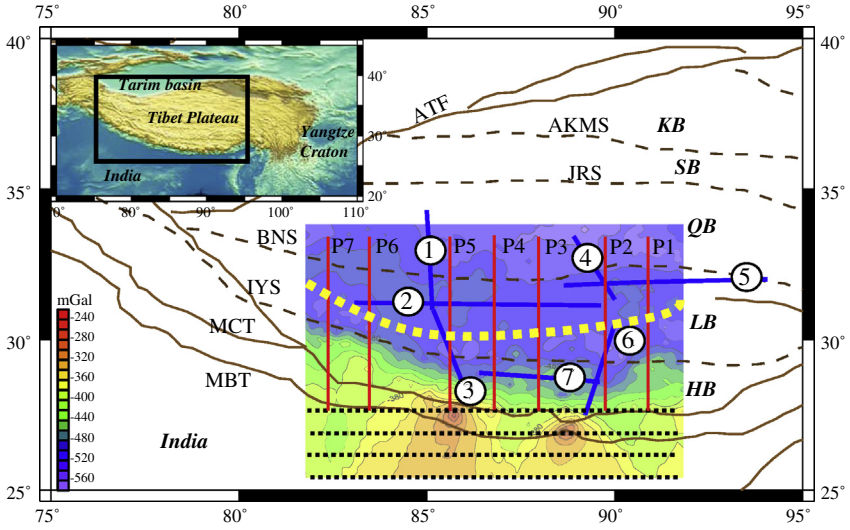

Fig. 1. Bouguer anomaly data of the central-south Tibet. The black dotted lines mark the area where the terrestrial gravity data are unavailable. The yellow curve connects a series of gravity lows, which are placed above the supposed northern margin of the Indian plate. Blue curves present location of studied seismic and seismological profiles. Seismic lines 1, 2, 3, 4, 6 and 7 are used in gravity modeling. Red lines indicate the vertical planes used to construct the geometry and initial density structure of the 3-D model. (For interpretation of the references to color in this figure legend, the reader is referred to the web version of this article.)

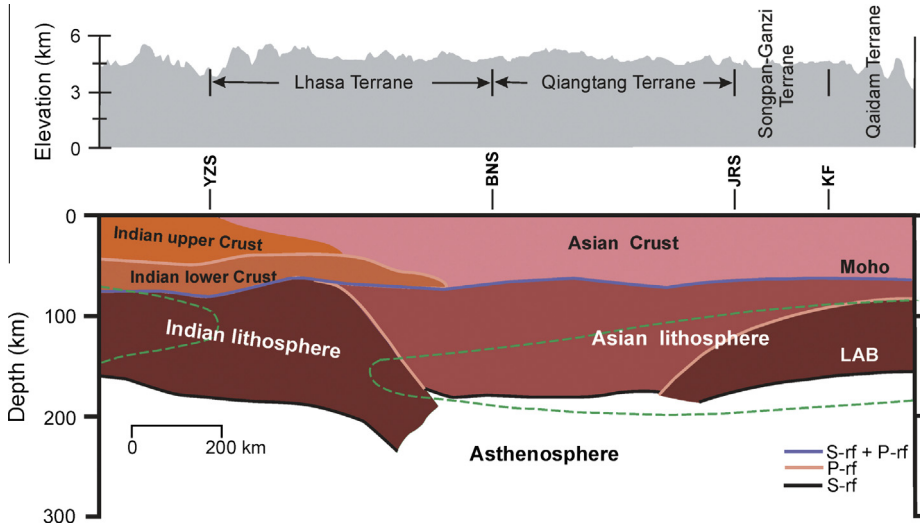

Fig. 2. Sketch map of the collision of the Indian and Asian lithospheric plates from the results of S receiver function (S-rf) analysis and P receiver function (P-rf) results (after Kumar et al. (2006)).

the GRACE potential field (Shin et al., 2007) which is combined with the satellite derived gravity field and terrestrial gravity data.

From Fig. 1, we can observe that the Bouguer anomaly varies between −574 mGal and −247 mGal in the study area. The difference reaches 327 mGal, which indicates large-scale variations in the crustal structure of the area. An extensive gravity low (longitude 86–92°E and latitude 32–34°N) is located in the north-east of the study area. Three limited gravity lows are located in the Lhasa block, around (83°E, 31°N), (86°E, 30°N) and (90°E, 30°N), respectively. The gravity data along seven ~1000 km long profiles give similar trends with a ~500 mGal Bouguer anomaly decrease from the Himalaya crossing southern Tibet to the central Tibet.

3. Procedure and initial 3-D crustal density model

3.1. Modeling technique

Forward modeling of the Bouguer anomaly was performed using the IGMAS software (Interactive Gravity and Magnetic Application System; see http://www.gravity.uni-kiel.de/igmas). The modeling software (Götze, 1984; Götze and Lahmeyer, 1988; Schmidt and Götze, 1998; Breunig et al., 2000) makes use of an interoperable 3-D Geoinformation System (IOGIS) and its functionality. The model is formed by 3-D bodies that are constructed using polyhedrals whose geometry is predefined by the user on a series of parallel vertical cross-sections, the 3-D structure is achieved in IGMAS by defining several vertical planes on which geological bodies are geometrically defined in the form of polygons. The vertical planes are connected via triangulation, thereby forming the 3-D structure. The geometry of the geological bodies is defined along the 2-D cross-sections, whereas the geometry in the area between them is interpolated. Hence, in order to perform more detailed modeling, a great number of 2-D cross-sections must be included.

The starting model of the density structure follows the geometry of the seismic results and is defined by nodal points (with x, y, z-coordinates and density values) within cross sections arranged parallel to each other and covering the study area. The nodal points

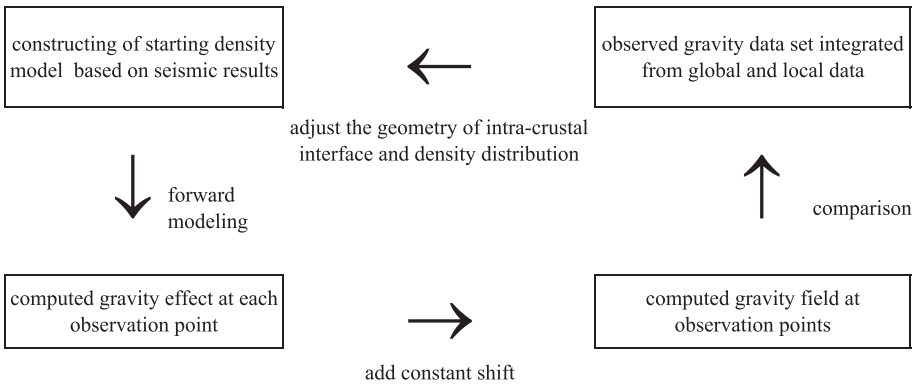

Fig. 3. Flow chart of gravity modeling process of crustal density structure.

define lines separating the density bodies within a certain cross section. The nodal points of corresponding lines within neighboring cross sections are automatically connected by triangulation, giving the surfaces of the density bodies. As another input, we have used the gravity data with a grid data file. In the southern most part of the profiles, the Chinese gravity data are unavailable but have been integrated with published global data sets (Shin et al., 2007). In order to retain the measured information, the gravity effect of the modeled structures is calculated at the measurement points. The design of a 3-D density model in IGMAS incorporates three important decisions: the definition of the initial structure, the selection of density values for the bodies forming the model and the choice of a reference model.

Fig. 3 shows the flow-chart of gravity modeling process of crustal density structure. The gravity effect of each 3-D (polyhedral) body is computed and added to the effect of the other ones, giving the anomaly value of the model structure for a given observation point. Generally, the observed and computed gravity fields do not agree. To enable the comparison between the two fields, a constant shift value is automatically determined and added to the computed anomalies (Fig. 3).

Initial density values for the modeled bodies are defined prior to the gravity modeling. By iteratively changing the geometry of the initial structure in accordance with the available constraining data incorporated in the IOGIS, the optimal fit between the observed Bouguer anomaly and the anomaly produced by the modeled 3-D density structure is achieved. This modeled anomaly is calculated from the density contrast between the modeled bodies and a layered background reference model.

3.2. Construction of initial 3D density structure model

The initial density structure is constructed with a priori information from wide-angle seismic reflections, receiver functions, and tomography acquired in the study area.

An initial crustal model is constructed by compiling available seismic and other geophysical data. The degree of freedom in modifying the geometry of the crustal layers depends on the availability and quality of seismic data. The study area was modeled with 7 south–north oriented and c.a. 900 km long cross-sections, with spacing interval of 1° or 2° (Fig. 1). From east to west, the model structure is c.a. 1000 km wide. To suppress edge effects, the density model was extended in all directions with the last given values for up to 1500 km. Depth extension is 260 km. None of the sections runs parallel to one of the seismic lines, but crosses them.

As it is well known, the greatest density contrast in the lithosphere is located at the Moho interface, followed by the sediment–basement interface. Previous works (Jin et al., 1996; Braitenberg et al., 2000) have estimated the gravity effect of lithospheric thickening and have shown that over the Tibet plateau the gravity effect is almost constant, with variation of about 10 mGal. Although the effect of the lithospheric thickening is very small, as the density contrast of the lithosphere to the asthenosphere (assumed as 0.03 g/cm^3) is less than one tenth of the value at the Moho (Shin et al., 2007), the asthenosphere layer is still considered in the modeling of this study.

Kumar et al. (2006) presented a high-resolution image of the base of the lithosphere from S-to-P converted seismic waves, revealing the collision architecture of the Indian and Asian continental plates beneath the Tibet Plateau. The base of the Indian

Table 1
Physical parameters of the different bodies used in the initial modeling.

Description	ρ (g/cm^3)	V (km/s)
Tertiary Indian foreland basin	2.45	Vs = 2–2.75 (Mitra et al., 2005)
India UC-lesser Himalayan	2.7–2.89	Vs = 3.5–3.8 (Mitra et al., 2005)
Greater Himalayan belt	2.75–2.91	Vs = 3.4–3.8 (Mitra et al., 2005) Vp > 5.7 (Hauck et al., 1998)
Tethyan Himalayan sequences	2.65–2.7	Vs = 2.5–3.2 (Mitra et al., 2005) Vp = 5.2 (Hauck et al., 1998)
Gangdese Batholith	2.75	
Lhasa block UC	2.7–2.93	Vp = 6–6.5 (Meissner et al., 2004) Vp = 6.1–6.5 (Zhao et al., 2001)
Qiangtang Basin, sediments	2.5–2.6	Density (Haines et al., 2003) Vp ~ 5.7 (Meissner et al., 2004)
Qiangtang block UC	2.64–3.01	Density (Haines et al., 2003) Vp ~ 5.8–7 (Meissner et al., 2004) Vp ~ 5.6–6.5 (Zhao et al., 2001)
Songpan–Ganzi terran, Kunlun	2.6–2.85	Vp = 5.4–6.2 (Jiang et al., 2006)
Qaidam Basin	2.4	Vp = 5–5.5 (Zhao et al., 2006)
Qaidam–Qilian Shan UC	2.53–2.92	Vp = 6–6.3 (Jiang et al., 2006) Vp = 5.5–6.5 (Zhao et al., 2006) Vp = 5.5–6.3 (Gao et al., 1999)
India LC	2.98	Vs = 3.9 (Mitra et al., 2005)
Greater Himalayan LC	3.05	Vs = 4–4.2 (Mitra et al., 2005)
Lhasa–Qiantang LC	3.05	Density (Haines et al., 2003) Vp = 6.6–7.1 (Meissner et al., 2004) Vp = 7–7.3 (Zhang and Klemperer, 2005) Vp = 6.5–7.3 (Zhao et al., 2001)
Qaidam–Qilian–Beishan LC	3.0	Vp = 6.5–6.8 (Jiang et al., 2006)
Lithospheric mantle	3.2	

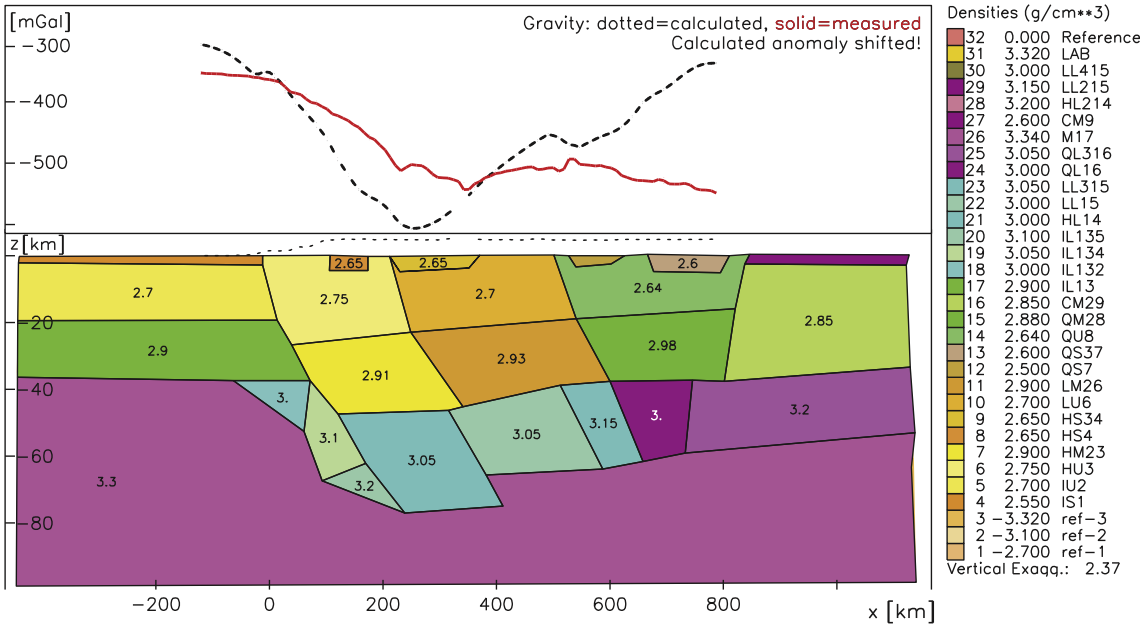

Fig. 4. The eastern cross-section of the initial model. Densities are deduced from P-wave velocity following Table 1.

Table 2
Physical parameters of the different bodies used in the density modeling.

Unit	ρ (g/cm^3)	Vp (km/s)	Temp. (°C)	Vp′ (km/s)
IS1	2.55	3.59–4.6	50–150[a]	3.72–4.75
IU2	2.7	5.9–6.5	150–250[a]	6.04–6.64
HU3	2.75	>5.7 (Hauck et al., 1998)	<400	>5.88
HM23	2.9	6.5	<600[a,c]	6.69
HS4	2.65	4.2–5.3	50–180	4.32–5.45
HS34	2.65	4.2–5.3	50–180	4.32–5.45
LU6	2.7	6–6.5 (Meissner et al., 2004; Zhao et al., 2001) 6–6.25 (Haines et al., 2003)	<600[c]	6.2–6.69
LM26	2.9	6.5–6.73 (Haines et al., 2003) 6.5–6.7 (Meissner et al., 2004)	800c	6.69–6.85
QS7	2.5	4–5 (Haines et al., 2003)	<200b	4.13–5.15
QS37	2.6	4–5 (Haines et al., 2003)	<200 b	4.13–5.15
QU8	2.64	~5.8–6.2 (Meissner et al., 2004) ~5.6–6.5 (Zhao et al., 2001) 5.7–6.1 (Haines et al., 2003)	200–600[a,c]	5.76–6.77
QM28	2.88	6.65–6.85 (Haines et al., 2003)	800 c	6.95–7.11
IL13/132/134/135	2.9/3.0 3.05/3.1	6.7	350–450[a,c]	6.9
HL14/214	3.0, 3.2	6.9–7.3	700–800b	6.97–7.44
LL15/215	3.0, 3.15	6.6–7.1 (Meissner et al., 2004) 7–7.3 (Zhang and Klemperer, 2005) 6.5–7.3 (Zhao et al., 2001)	1000–1100[b] 700–800[c]	6.8–7.2
LL315	3.05	6.6–7.1 (Meissner et al., 2004) 7–7.3 (Zhang and Klemperer, 2005) 6.5–7.3 (Zhao et al., 2001)	1000–1100[b] 700–800[c]	6.8–7.2
QL16	3.0	6.6–7.1 (Meissner et al., 2004) 7–7.3 (Zhang and Klemperer, 2005) 6.5–7.3 (Zhao et al., 2001) 7.1 (Haines et al., 2003)	1000–1100[b] 700–800[c]	6.8–7.2

Descriptions of each unit: IS1 – Indian foreland basin; IU2 – Indian upper crust; HU3 – Himalaya upper crust; HM23 – Himalaya middle crust; HS4 – Himalaya sediments; HS34 – north Himalaya sediments; LU6 – Lhasa block upper crust; LM26 – Lhasa block middle crust; QS7 – Qiangtang block sediments; QS37 – north Qiangtang block sediments; QU8 – Qiangtang upper crust; QM28 – Qiangtang middle crust; CM29 Qaidam middle crust; IL13, IL132, IL134, IL135 – Indian lower crust; HL14 – Himalaya lower crust; LL15 – Lhasa block lower crust; LL315 –north Lhasa block lower crust; QL16 – Qiangtang lower crust; QL316 – Qaidam lower crust; M17 – upper mantle; CM9 –Qaidam upper crust. Black body texts for Vp are deduced from Vs from Mitra et al. (2005).

[a] Brewer et al. (2003).
[b] Jimenez-Munt et al. (2008).
[c] Hetenyi et al. (2007).

lithosphere dips northward from a depth of 160 km beneath the Himalayas to a depth of 220 km just south of the BNS. The base of the Asian lithosphere is nearly horizontal at the depth of 160–180 km from central to northern Tibet. There is a vertical gap of about 50 km between Indian and Asian lithospheres. Similar subduction images along two N–S profiles across the Tibetan plateau

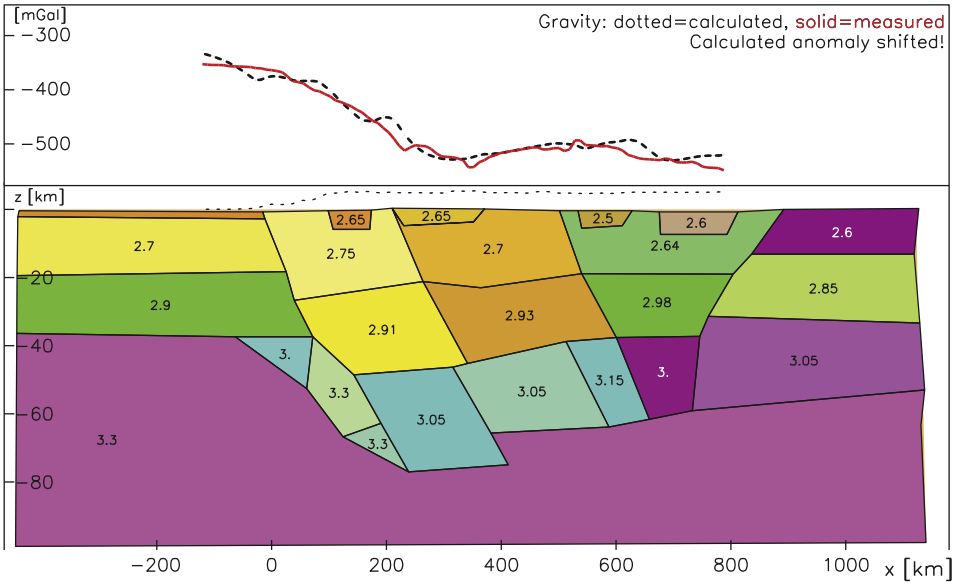

Fig. 5. The eastern cross-section of model II. Density of some units and the geometry of interfaces have been changed with respect to model I.

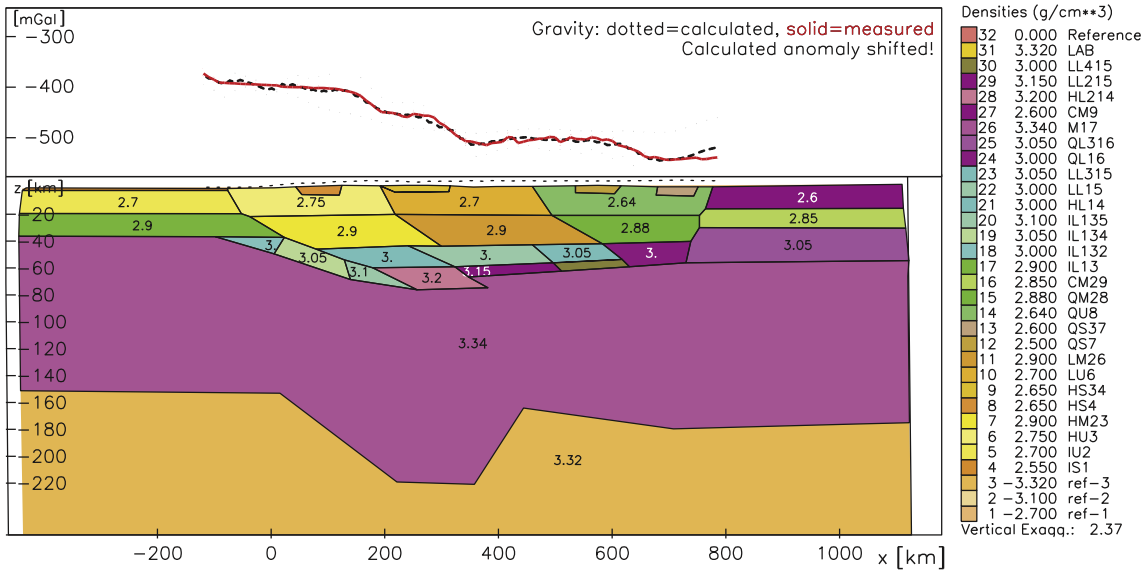

Fig. 6. The final constructed lithospheric density profile of model III.

have been disclosed by Chen et al. (2009a,b), which shows that the leading edge of underthrusting might have exceeded the BNS and, more to the north, even the JS (Jinsha Suture). Moreover, Chen et al. (2009a,b)'s results also indicates that the lithospheric root can be substantiated at ~180 km in some places (Qiangtang Block) and exceptionally at in some places (Lhasa Block). Fig. 2 shows the subduction of both the Indian and Asian lithospheres. The Indian plate is penetrating into the mantle to the south of the Bangong suture (BNS). This lithospheric model will be used in our gravity modeling for the constraint of the lithosphere–asthenosphere boundary.

Crustal structures in the studied area are constrained by wide-angle seismic profiles (Hirn et al., 1984a,b; Teng et al., 1980a,b; Xiong et al., 1985; Wu et al., 1993; Makvosky et al., 1996; Zhao et al., 2001; Zhang and Klemperer, 2005, 2010; Zhang et al., 2010). Seismic data provide valuable information not only on the geometry of crustal layers, but also on the depth distribution of P-wave velocities. In order to construct an initial density model, south–north trending velocity profiles have been collected from: (1) two deep seismic sounding profiles: Cuoqin-Sangehu (line 8), Zhangmu-Cuoqin (line 16); (2) three near vertical deep seismic reflection profiles of INDEPTH project: Yadong-Namucuo (line 1) from INDEPTH I and II (Makovsky et al., 1996), Deqin-Longwei Cuo (line 10) from INDEPTH III (Zhao et al., 2001); (3) two east–west trending velocity profiles, Paiku Tso-Puma Yum Tso (Zhang et al., 2002; Zhang and Klemperer, 2010) (line 2) and Siling Tso-Ya'anduo (Zhang and Klemperer, 2005) (line 3), will also be used to constrain the initial model and evaluate the final density model. (4) A 2-D velocity profile with 400 km length located in 30.8–34.1°N and 84–85.2°E had been studied by wide-angle reflection seismics (Xiong and Liu, 1997). (5) In the summer of 1998, project INDEPTH III recorded a 400 km length NNW–SSE wide-angle seismic profile in central Tibet, from the Lhasa block across the BNS at about 89.5°E and into the Qiangtang block. (6) Based on wide-angle reflection/refraction seismic survey, Zheng and Yao

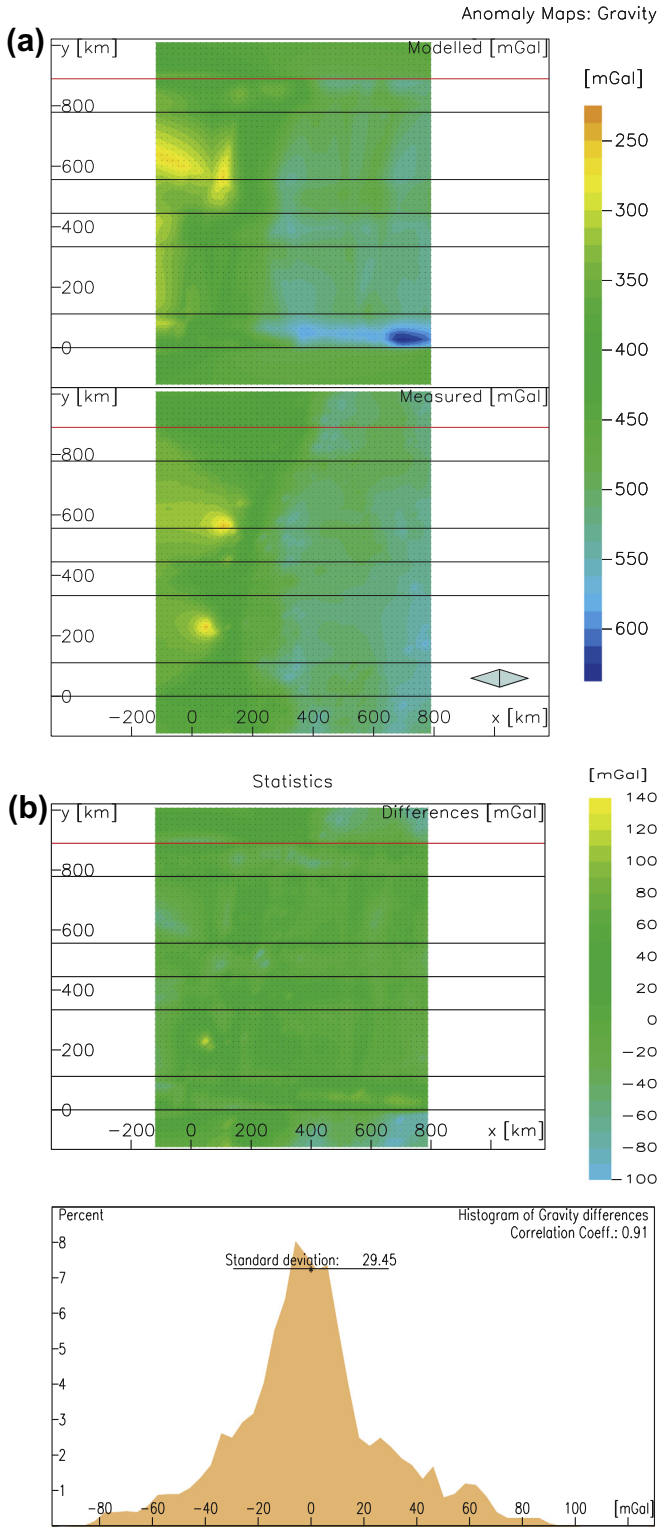

Fig. 7. (a) Observed and calculated gravity anomalies for model III in the study area. (b) Mismatch between observed and calculated anomalies and histogram of gravity difference. Black lines still indicate the vertical planes used to construct the geometry of the 3-D model.

(2004) proposed a profile (line 16) from Zhangmu to Cuoqing in southwest Tibet. (7) Another velocity model along seismic line 1 is obtained by reprocessing the INDEPTH I and II data using the ray tracing modeling method (Li, 2003).

The entire above seismic wave velocity interpretations are incorporated in this work in the process of constructing the 3-D gravity model for the transition zone between the Indian plate and the Eurasia plate. The modeling of potential fields will not only provide a more complete understanding of the crustal architecture, but also try to infer the physical properties and possible composition of anomalous crustal materials.

Initial crustal densities have been calculated at some sites along 7 north–south trending profiles from the proposed seismic velocities (Vp and Vs) and using the velocity–density relation of Christensen and Mooney (1995). The values of the physical properties considered for each body are listed in Table 1. The initial density model structure is taken from the seismic structure as given at these cross points. The western part of studied area (to the west of 86°E) is best controlled by the seismic line 1 and 3 (Fig. 1). The eastern part (to the east of 86°E) is weakly controlled by the seismic line 4 and 6, i.e., the initial density profiles are constructed following four seismic lines (line 1, 3, 4 and 6): the northern parts of profiles p1–p4 are controlled by line 4, the southern parts of p1–p4 by line 6; the northern parts of p5–p7 are controlled by line 1, the southern parts of p5–p7 by line 3.

4. Modeling process and final crustal density structure

As mentioned above, Fig. 3 shows the gravity modeling process of crustal density structure. Firstly an initial crustal model (model I, Fig. 4) based mainly on available seismic data was constructed to start the lithosphere modeling. The gravity anomaly was calculated for the initial density structure (Fig. 4) according to the relationship between velocity and density shown in Table 2. The gravity stations are placed at their measurement heights above sea level, but the topographic relief was not included in the model because its effect on the gravity attraction was already subtracted by the Bouguer and terrain corrections. The modeling result shows that the initial density model does not match the observed data completely. It demands further modeling by adjusting geometry of interfaces and inverting densities iteratively. In the initial model, the unit QL316 (Qaidam lower crust) should be noticed for its high density value (3.2 g/cm^3). Since seismic and seismological investigations have proposed a thick crust over 40 km and unit QL316 is located in the lower crust, the density of unit QL316 should be decreased in order to match the gravity field. The optimal value is estimated to be 3.05 g/cm^3. In order to fit the observed Bouguer anomaly data, the interfaces have been changed by less than 2 km.

With the adjustment of geometries of intra-crustal interfaces, we get a model II (Fig. 5) with which the calculated Bouguer anomaly is in good agreement with the observed data with the exception of some misfits that are either local or at the border of the model. The main negative anomalies of the contact zone between the Indian and Eurasia plates are properly reproduced. The residuals of observed and calculated Bouguer anomalies are around zero with a standard deviation of 31.4 mGal, which is 5.4% of the maximum Bouguer anomaly (−580 mGal) and the correlation coefficient is 0.9 between the observed and calculated Bouguer anomaly. We then get the final crustal density model (model III, Fig. 6) until fitting the calculated and the observed Bouguer anomaly dataset by adjust density distribution with the fixed geometry of the crustal structure in model II (Fig. 5).

Usually, the accuracy of the 3-D density model presented is quantified in terms of how well it reproduces the observed gravity anomalies. However, this does not say anything about the validity of the modeled structures, particularly in the areas where no other geophysical data are available. Due to the non-uniqueness of the interpretation of potential field, other models with different structure and density distribution could also reproduce the observed anomalies with the same accuracy, although they would be hardly

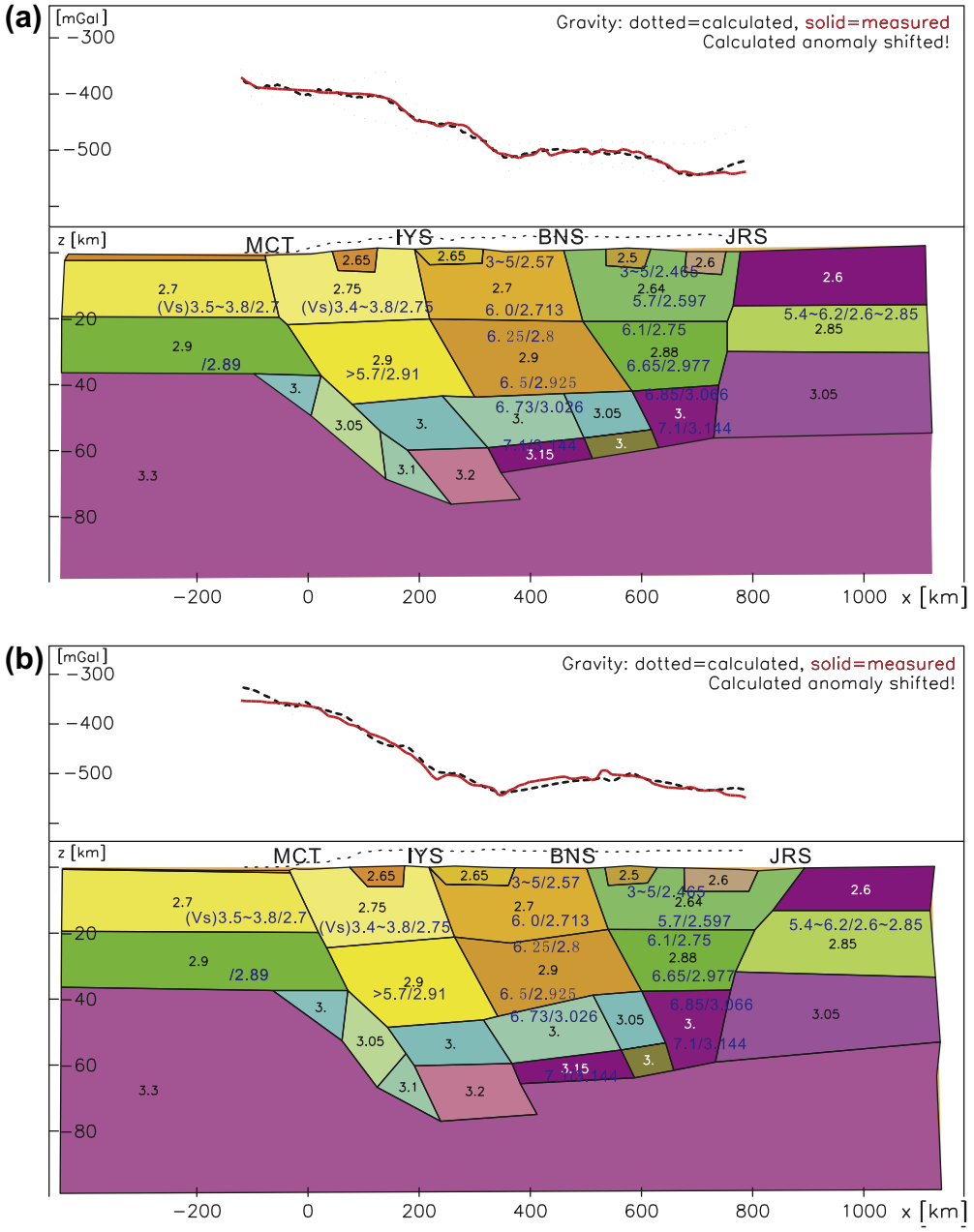

Fig. 8. (a–g) Cross-sections P1–P7 (Fig. 1) of the final density model (model III). IS1 – Indian foreland basin; IU2 – Indian upper crust; HU3 – Himalaya upper crust; HM23 – Himalaya middle crust; HS4 – Himalaya sediments; HS34 – north Himalaya sediments; LU6 – Lhasa block upper crust; LM26 – Lhasa block middle crust; QS7 – Qiangtang block sediments; QS37 – north Qiangtang block sediments; QU8 – Qiangtang upper crust; QM28 – Qiangtang middle crust; CM29 Qaidam middle crust; IL13, IL132, IL134, IL135 – Indian lower crust; HL14 – Himalaya lower crust; LL15 – Lhasa block lower crust; LL315 – north Lhasa block lower crust; QL16 – Qiangtang lower crust; QL316 – Qaidam lower crust; M17 – upper mantle; CM9 – Qaidam upper crust.

probable, due to the fact that continuity of the crustal structure and of its layers exists. The further evaluation of the model needs integration with reliable geological and geodynamical information. Due to the fact that densities in the middle and lower crust are higher than global average values, eclogitization will be discussed in the next section.

Fig. 6 illuminates our preferred model (model III) after several tests following a trial-and-error approach. The calculated Bouguer anomaly is in good agreement with the observed data, with the exception of few local misfits (Fig. 7). A comparison between the observed and calculated gravity anomaly maps over the 3-D model is shown in Fig. 7a). The main negative anomalies of the contact zone between the Indian and Eurasia plates are properly reproduced like in model II. The histogram (Fig. 7b)) shows a tight concentration of residuals around zero with a standard deviation of 29.45 mGal, 5.1% of the maximum Bouguer anomaly (−580 mGal) and correlation coefficient is 0.9 between the observed and calculated gravity anomaly data.

In the above-mentioned way, we get the final crustal density structures along seven North–South profiles (Fig. 8a–g). The density model can be summarized as: density is about 2.7 g/cm^3 beneath Indian plate, and 2.75 g/cm^3 beneath Himalaya block, and 2.7 g/cm^3 beneath Lhasa block, 2.64 g/cm^3 beneath Qiangtang block and 2.5 g/cm^3 beneath the Songpan-Ganzi block. In the middle and lower crust, density is about 2.9 g/cm^3 beneath Indian plate, 2.9–3.2 g/cm^3 beneath Himalaya block, and 2.9–3.05

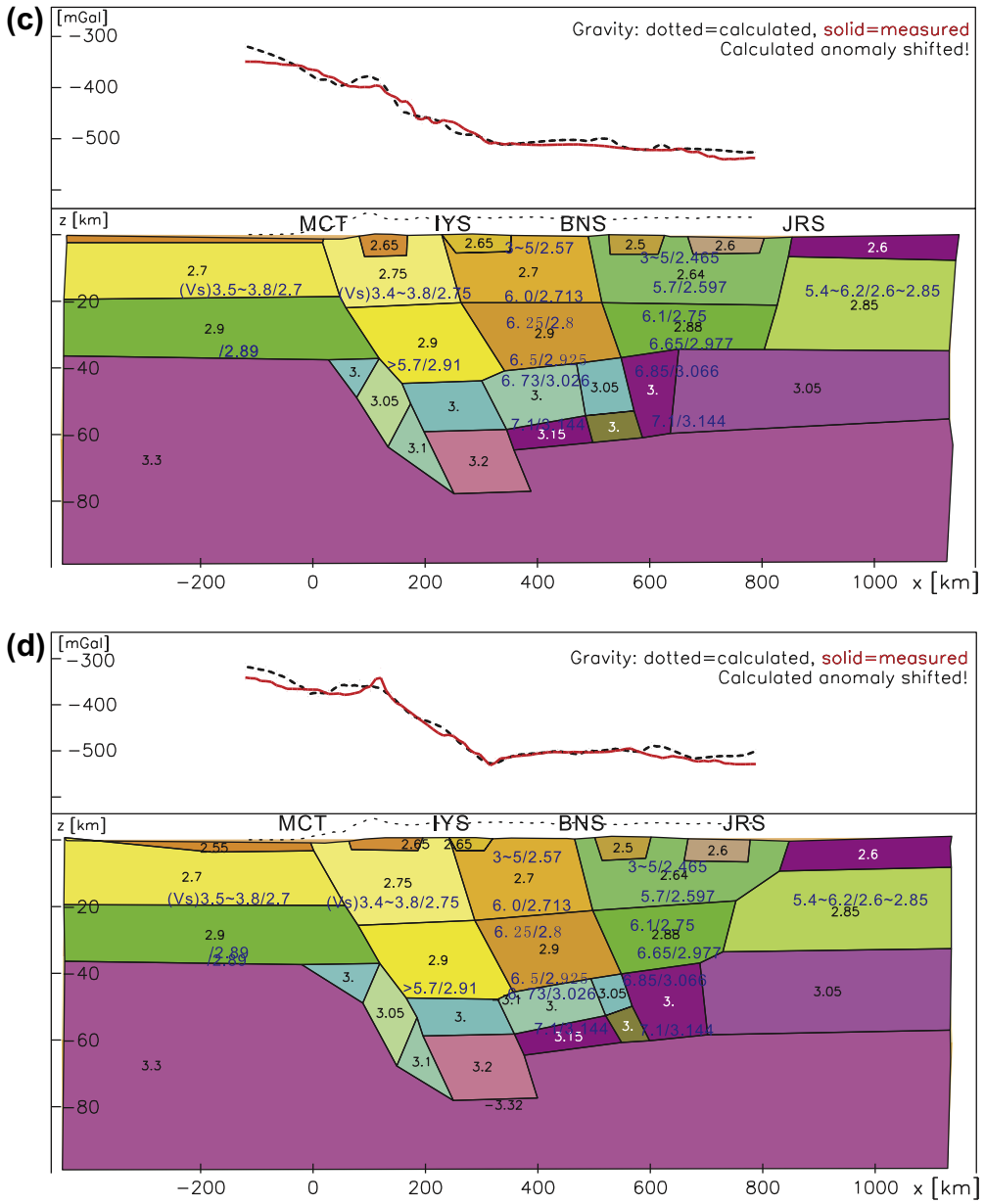

Fig. 8. (*continued*)

beneath Lhasa terrane, 2.88–3.0 g/cm^3 beneath Qiangtang block, 2.85–3.05 g/cm^3 beneath Songpan-Ganzi block (Table 3).

For the crustal thickness beneath the south of IYS, it is deeper than70 km beneath the Himalaya block with Moho depth of 73–79 km and the average Moho of 76 km beneath the eastern profiles. Moho depth ranges within 70–78 km with the average of 73 km beneath the west profiles.

Crustal thickness beneath Himalaya block becomes less from east to west and declines northward, with a crustal thickness of 78 km in the east (Pumoyong Cuo, the distance is 70 km along Yadong-Namu Cuo profile) and about 70 km in the west (Peigu Cuo).

Moho deepens northward, but displays as a non-constant offset beneath the sutures from the eastern to the western profiles. Usually in the south of IYS, the depth of Moho interface is deeper in the east than the west as Moho interface is at depth of 73–79 km with the average of 76 km in the east; but 70–78 km and the average of 73 km in the west. A complex undulated Moho exhibits beneath the sutures and the Moho declines northward entirely in the east.

5. Discussion

A 3-D crustal model has been derived for the transition zone between the Indian plate and the Eurasia plate beneath Tibet. The model is seismically constrained and explains the main gravity anomalies over the area. The tectonic implications of this study are discussed hereafter.

5.1. Checking of the model by comparison with other geophysical data

Fig. 9 displays the comparison of our crustal density model with crustal structures from other related geophysical observations (Yuan et al., 1997; Zhao et al., 2001; Zhang and Klemperer, 2005). From the figure, we can observe that the boundaries between the density layers of the model match well with the interfaces of the shear wave velocities gradient. The crustal velocities are from INDEPTH III (Zhao et al., 2001) and density was calculated

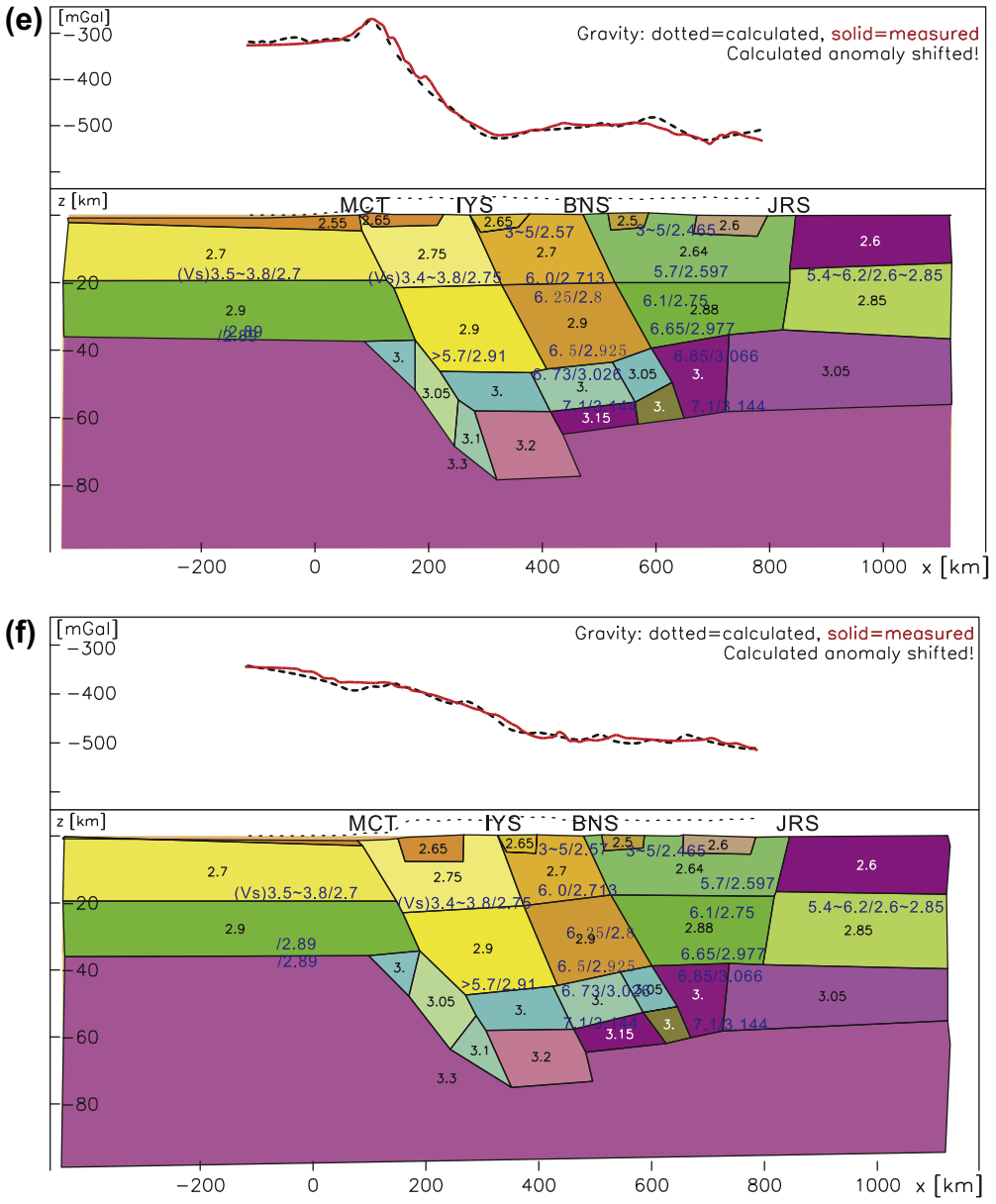

Fig. 8. (*continued*)

using the velocity–density regression parameters of Christensen and Mooney (1995). The average Moho depths of Lhasa block and Qiangtang block in model III are close to the result of INDEPTH III experiment. The modeled densities are slightly lower than those deduced from the velocity–density regression parameters. Comparing the modeled structure with an east–west profile (Zhang and Klemperer, 2005), which intersects the velocity profile at 260 km, which corresponds to 435 km position of the density profile, we find that the offsets are less than 4 km. the interfaces of the top of the lower crust and Moho have 2 km offset with respect to the result of the receiver function (Yuan et al., 1997). Through the sensitivity test of gravity modeling, we find that the anomaly is not sensitive to the 2 km offset in the depth of ~70 km. So this offset is negligible when applying the gravity method.

5.2. Lateral variation of the Indian plate subduction angle

The role of the Indian crust in doubling the thickness of the Tibetan crust is still a subject of debate. Makovsky et al.'s (1996) results tightened the geometrical constraint on the northern extent of the Indian crust. Three alternative conceptual models for the northern extent of Indian crust were discussed under the hypothesis that the Indian crust remains intact with a thickness of 30–40 km and that it penetrates north of the Tethyan Himalaya (Argand, 1924; Powell and Conaghan, 1973; Ni and Barazangi, 1984; Allègre et al., 1984; Harrison et al., 1992; Dewey and Burke, 1973; Molnar, 1988). The first one is that the Indian crust flattens and underthrusts Asian crust to produce the double-thickness Tibetan crust (Argand, 1924; Powell and Conaghan, 1973; Ni and Barazangi, 1984). The second model assumes that the Indian crust continues to dip to the north at the observed 7–10°, or only gradually steepens, and so underthrusts the IYS within the lower crust for about 100 km to the north but does not constitute the lower half of the Tibetan crust through central and northern Tibet (Allègre et al., 1984; Harrison et al., 1992). In the last model the Indian crust is subducted into the mantle south of the IYS and does not constitute a part of the Tibetan crust (Dewey and Burke, 1973; Molnar, 1988). Moreover, the tomography results of shear wave

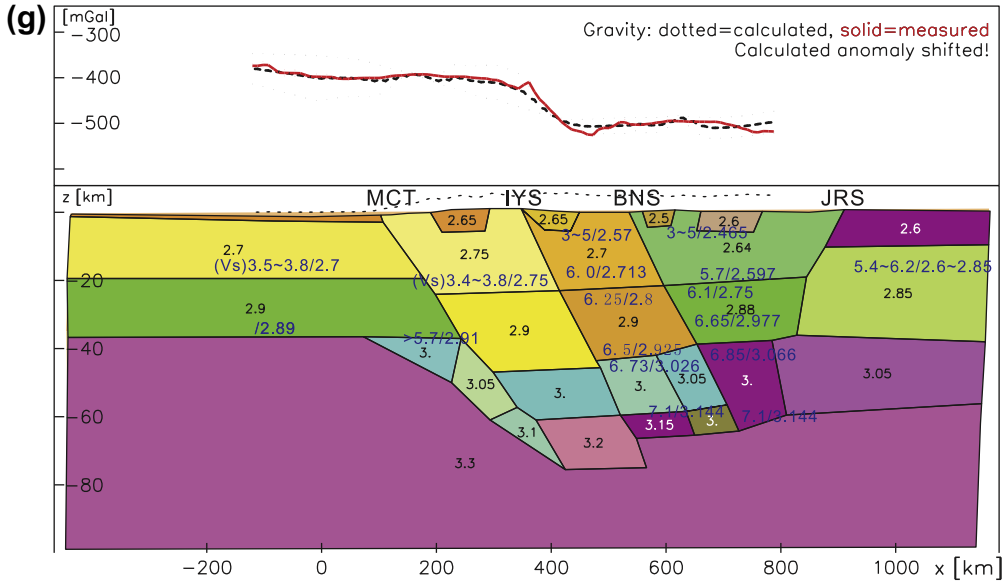

Fig. 8. (*continued*)

Table 3
Final crustal density structure along seven N–S profiles.

Block	Layer	Density (g/cm^3)
Indian	Upper crust	2.7
	Middle-lower crust	2.9
Himalaya	Upper crust	2.75
	Middle-lower crust	2.9–3.2
Lhasa	Upper crust	2.7
	Middle-lower crust	2.9–3.05
Qiangtang	Upper crust	2.64
	Middle-lower crust	2.88–3.0
Songpan-Ganzi	Upper crust	2.5
	Middle-lower crust	2.85–3.05

velocity given by Chen et al. (2009a) shows that the leading edge of underthrusting might have exceeded the BNS and, more to the north, even the JS (Jinsha Suture). Obviously, the Indian plate subduction angle is another important information to constrain the behavior of the Indian plate subduction.

The geometric constraints given by the INDEPTH-I wide-angle seismic reflection survey excludes the possibility of models 1 and 3. Therefore model 2 is preferred and it suggests that the Indian crust continues north of the Tethyan Himalaya and underthrusts the IYS within the lower crust. Makovsky et al. (1996) observed the Main Himalayan Thrust (MHT) continuing with a uniform dip of 7–10° to a depth of about 40 km beneath the surface at a distance of only 70 km south of the IYS where the Tibetan Plateau crust is 65–70 km thick. The interpretation of wide-angle seismic profile between Peigutso and Pumoyongtso in Tethys Hiamlaya declared the gentle Indian plate subduction of about 8.5–9°, but may endured a transition from steep subduction to nearly flat subduction (Zhang and Klemperer, 2010).

In addition, according to the Hetenyi et al.'s study (2007), the results of Hi-CLIMB experiment gave a more appropriate answer to the northward extent of the India plate: the plate margin is located parallel to the Himalayan arc, and about ~450 km north of the Main Frontal Thrust. In the meantime, the comparison of six images along four profiles shows that while the location where the Indian crust reaches its maximal depth can be approximately related to the Yarlung-Tsangpo Suture, the position of the Banggong-Nujiang Suture with respect to the northern extent of the Indian lower crust is variable, with horizontal distances ranging between 0 and 150 km.

Comparing the east and west cross-sections, the dip angle of the Moho interface is larger in the middle of the study area. The former is ~8.5° in the eastern and western areas, while is ~16.7° in the middle of the study area (Fig. 10). Hence the Indian plate collides with the Eurasia plate with a gentle angle of inclination in east and west, while steeper in the middle part.

Deep seismic sounding survey in the Kashmir Himalaya (Kaila and Narain, 1976) shows a Moho dipping toward the north–northeast direction, at an average angle of 15–20°. Hauck et al. (1998) and Schulte-Pelkum et al. (2005) proposed that the Moho dips with an angle of few degrees northwards beneath the Sub and Lesser Himalaya and steepens to about 15° beneath the greater Himalaya. Tiwari et al. (2006) suggested MBT and MCT dip with an angle of 22° and 16° to the north, respectively. Similarly, our gravity modeling shows that the Indian shield underthrusts the plate with a slightly steeper angle beneath the central part than beneath the eastern and western parts in central-south Tibet.

5.3. Moho undulation across the Yurlung-Zangpo suture belt

Tectonically, Yurlung-Zangpo suture belt records key process of the collision between the Indian and Eurasia plates at 50 Ma (Zhang et al., 2012 and references therein). But the penetration depth of the suture belt is still not definitively imaged in spite of the previous studies. Here, we use our solution to show a 3D Moho topography map across Yurlung-Zangpo suture belt. Fig. 11 shows the flexure of the Moho interface according to our model.

A seismic profile with 430 km length in central Tibet given by Teng et al. (1980a,b) along the north–south direction near longitude 90°E provided the most detailed information for the crustal structure at that time. Teng et al. (1980a,b) showed that the crust on two sides of the India-Yalunzambu suture (IYS) is significantly different. The crust is 70–73 km thick in the northern side of the IYS. A layer with P velocity of 6.0–6.2 km/s underlying a 4–5 km thick sedimentary layer, extends to a depth of about 45 km. A low-velocity layer of 5.6 km/s appears between the depth of 45 km and 55 km, underlain by a lower crust with about 7.2 km/s P wave velocity. The crust thins from 65 km to 45 km near

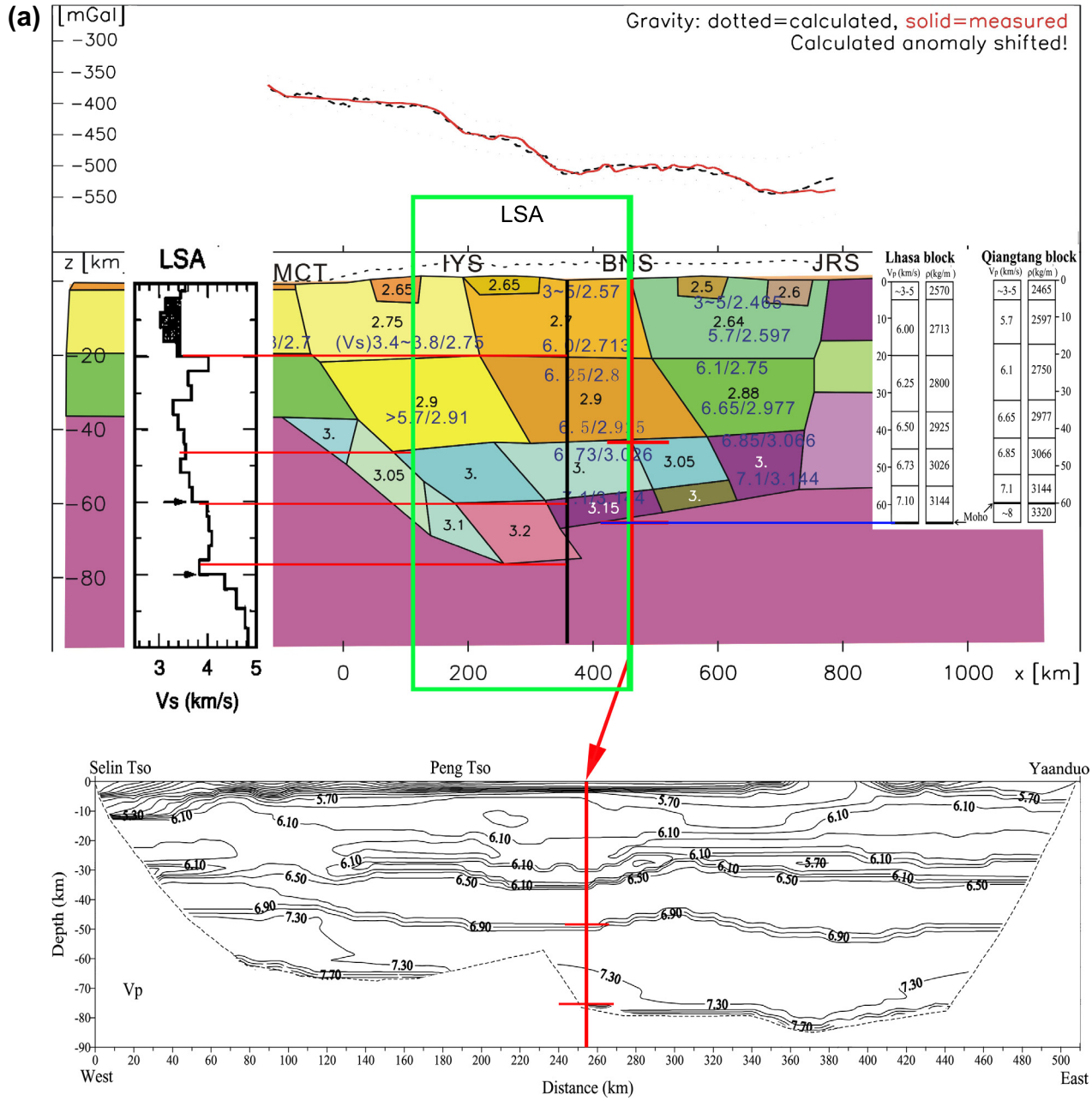

Fig. 9. Comparison of our crustal ensity model and related seismic results; (a) Basemap showing the modeled density structure of profile P1 (Fig. 8a) with black numbers as densities and blue numbers as the seismic-wave velocities and its deduced densities. Left inset (1) is a 1-D shear wave velocity (after Yuan et al. (1997)) for permanent station LSA using receiver function method. Right inset (2) is velocity (Vp) and density (ρ) columns for the Lhasa and Qiangtang blocks (after Haines et al. (2003)). Black line shows the referred position in inset (1); Green rectangle marks the area referred in inset (2). The bottom figure showing the 2-D east–west P-wave velocity profile of wide angle seismic reflection experiment (Zhang and Klemperer, 2005). Detailed explanation see text. (b) Basemap shows profile P2 (Fig. 1) of the modeled density structure, and the right Inset showing the 1-D velocity-depth function derived from the receiver function study (Yuan et al., 1997). (For interpretation of the references to color in this figure legend, the reader is referred to the web version of this article.)

Yadong in the south of IYS. In summary, the crust beneath the Himalaya is significantly thinner than the average crust in Tibet. The thinning of the crust continues southward to about 40 km under the Ganges Basin and to about 35 km under central India.

5.4. Crustal composition model of study area

Integrating crustal P-wave velocity distribution from wide-angle seismic profiling, geothermal data and crustal density model, the crustal lithologic composition model can be estimated (Zhang et al., 2008, 2009a; Zhao et al., 2012). With similar approach we infer a crustal composition model of study area, which is composed of an upper crust with granite–granodiorite and granite gneiss beneath the Lhasa block; biotite gneiss and phyllite beneath the Himalaya, a middle crust with granulite facies and possible pelitic gneisses, and a lower crust with gabbro–norite–troctolite and mafic granulite beneath the Lhasa block. The details of reconstructing this petrological model mentioned above will be presented elsewhere.

5.5. Evaluation of eclogitization in the lower crust

Eclogitization beneath Tibet is a subject of broad interest in the field of earth sciences. Previous studies suggest that that eclogitization of the lower crust probably play an important role in the

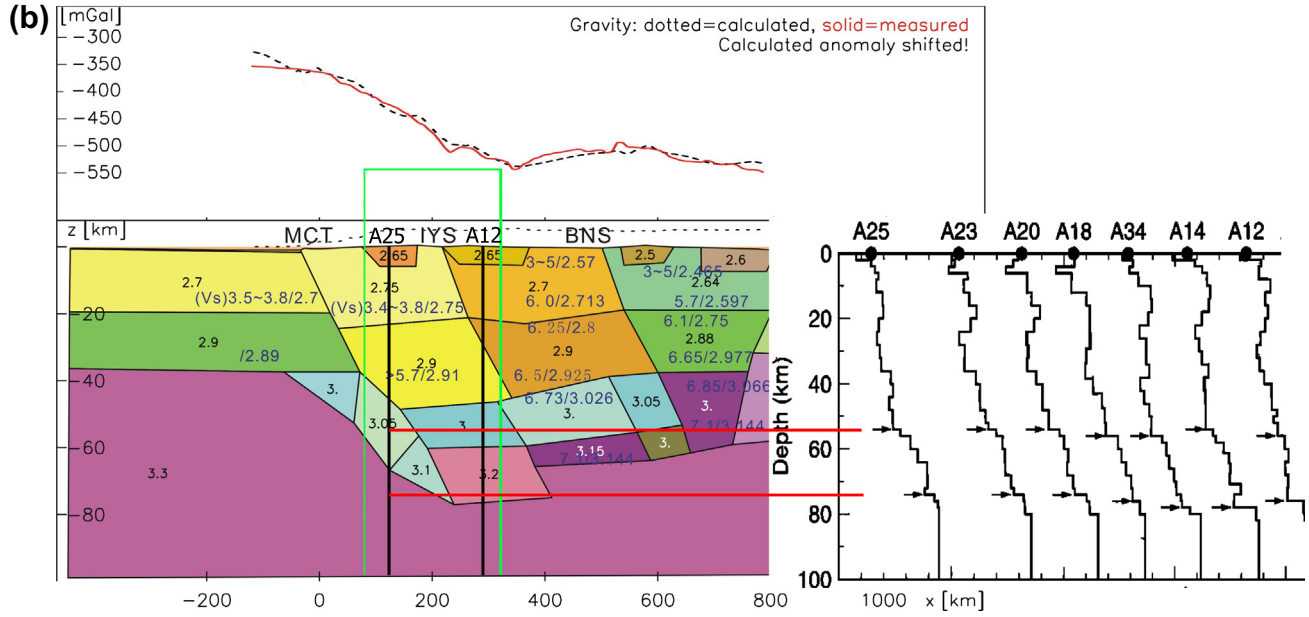

Fig. 9. (*continued*)

orogeny process of Himalayas and Tibet plateau (Bousquet et al., 1997; Henry et al., 1997; Cattin et al., 2001; Tiwari et al., 2006; Hetenyi et al., 2007). In the north of the Himalaya, the lower Indian crust is characterized by a high-velocity region consistent with the formation of eclogite and a high-density material whose presence affects the dynamics of the Tibetan plateau (Schulte-Pelkum et al., 2005). However, several seismic studies have inferred abnormally low, rather than increased, velocities for the Tibetan lower crust (Cotte et al., 1999; Zhao et al., 1996), suggesting an absence of eclogite. Gravity modeling will be an extra constraint on the absence or presence of eclogitization in this study.

An end-member model (Fig. 12) is designed with eclogite in the lower crust, with the same geometry as in model II. The calculated gravity anomaly is larger than the observed data, when using the model with lower crustal density over 3.3 g/cm^3 beneath the Himalaya and Lhasa block. In order to match the calculated gravity anomaly with the observed data, the lower crustal densities are reduced. Finally, model III is created and its average lower crustal density is less than 3.2 g/cm^3.

There are different opinions about the eclogitization in the lower crust of Tibet. The first one (Le Pichon et al., 1997; Schulte-Pelkum et al., 2005) supports the presence of eclogite beneath the Himalaya. Based on a receiver function study and observed fast P-wave velocities in the lower crust, Schulte-Pelkum et al. (2005) argue that the lower crust is partially (~30%) eclogitized just South of the IYS, and that the eclogitization process is governed by water availability. This implies that the lower-crust material reaches the eclogite facies via granulite facies conditions, as shown in Le Pichon et al. (1997) for geotherms established after more than ~20 My of relaxation. However, the latter study also shows that the geotherm may follow an amphibolite–eclogite and even a blueschist–eclogite path for shorter relaxation times between ~10–20 My and less than ~10 My, respectively.

Based on thermo-kinematic modeling, Henry et al. (1997) proposed that the high altitude of the Himalayas is related to the absence of eclogites beneath the mountain range. Eclogites would not have been formed due to the fast rates of underthrusting of relatively cold material.

The third opinion is in support of the ecologitization beneath Lhasa block (Tilmann et al., 2003; Cattin et al., 2001; Tiwari et al., 2006). Seismic tomography of the upper mantle in central Tibet revealed a subvertical high velocity zone beneath the northern Lhasa block (Meissner et al., 2004) that probably represents the front of the detaching of the Indian lithosphere (Tilmann et al., 2003). The tomography results of shear wave velocity given by Chen et al. (2009a) shows that the leading edge of underthrusting might have exceeded the BNS and, more to the north, even the JS (Jinsha Suture). It seems that the relative slow shear wave velocity anomalies within middle-lower crust (velocity slices at 45 km and 75 km) do not support the idea of ecologitization in lower crust beneath central-north Tibetan plateau. Furthermore, based on gravity data combined with numerical modeling, Cattin et al. (2001) showed that eclogitization does not take place under the High Himalayan range as expected from a steady-state local equilibrium assumption, but rather further North beneath the Tibetan Plateau. More recently, Tiwari et al. (2006) showed that gravity and magnetic anomalies across Sikkim can be explained with a model in which the crust beneath Tibet (between 56 and 72 km depth) is eclogitized ~100 km north of the IYS.

Mengel and Kern (1990) proposed that the P-wave velocity of eclogite in lower crust is 6.8–7.6 km/s and density is 3.15–3.6 g/cm^3. According to the modeled density structure, our result shows that the lower crustal densities are smaller than 3.2 g/cm^3 and suggests the absence of eclogite or partial eclogitization due to delamination under the central-south Tibet. Obviously, our crust density values and composition structure in the lower crust do not support the existence of eclogite in the lower crust beneath central-south Tibet.

6. Conclusion

The Himalaya and Lhasa blocks are the product of the deep-reaching process of mountain building due to the convergence and collision of the Indian and Eurasian plates. We define a 3D density model beneath these tectonic blocks constrained by a review of all available active seismic and passive seismological results on the velocity structure of the crust and lower lithosphere in Tibet.

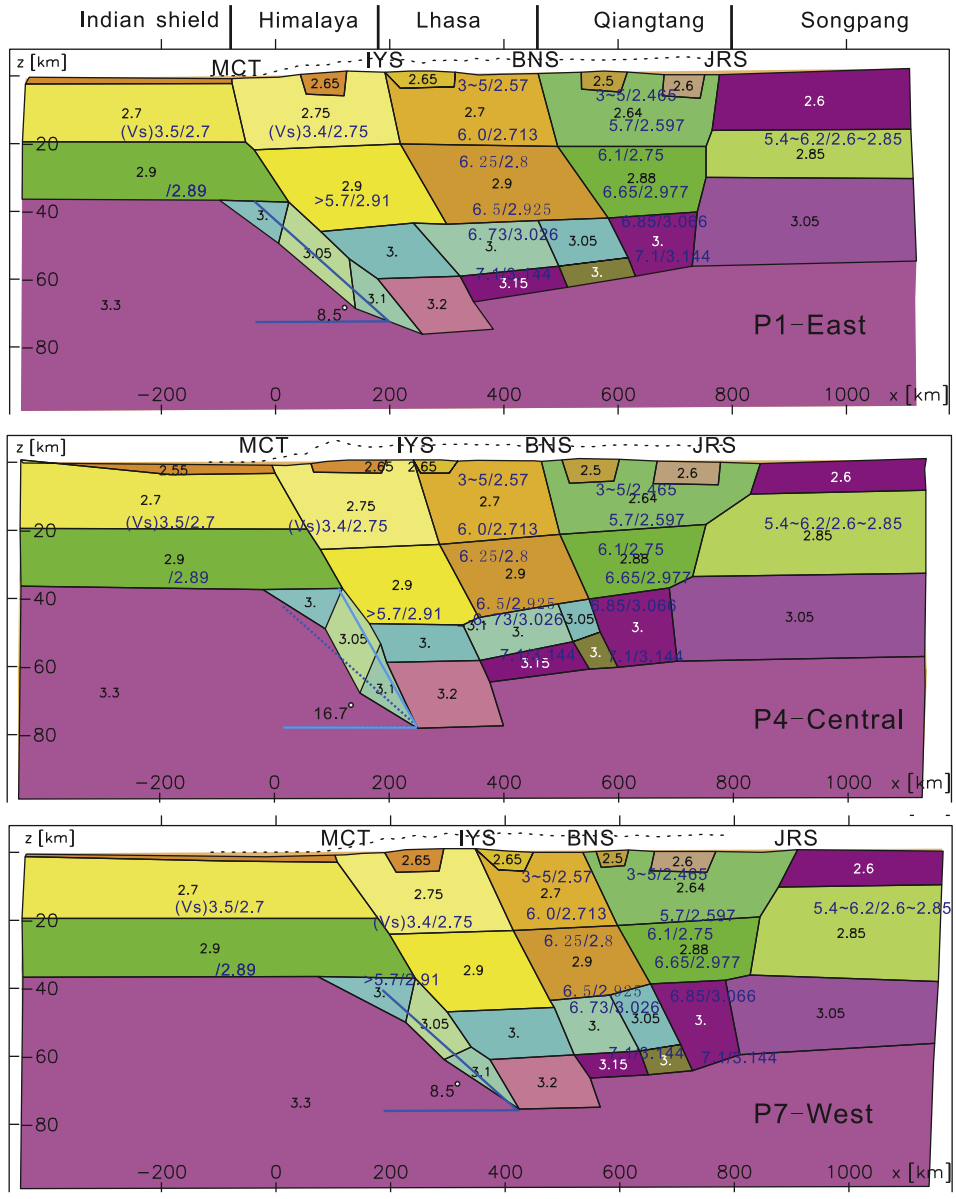

Fig. 10. Three profiles of model III. P1 stands for the eastern, P4 for the central and P7 for the western profile, respectively.

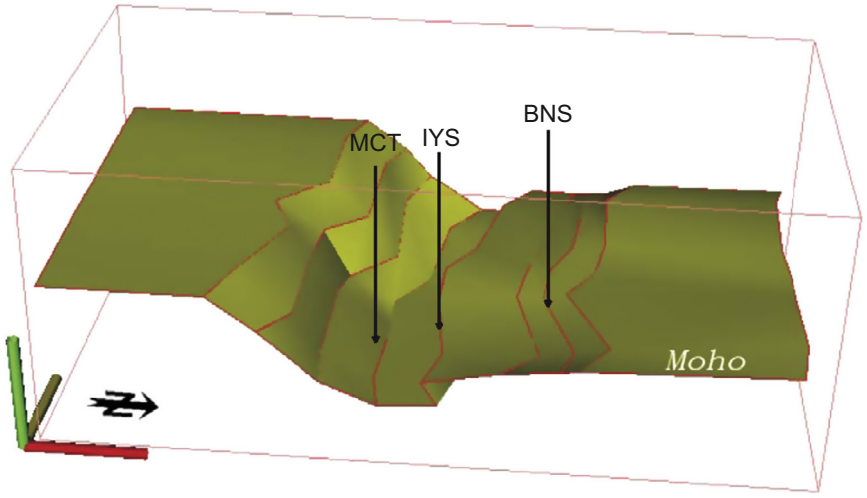

Fig. 11. Moho interface of model III.

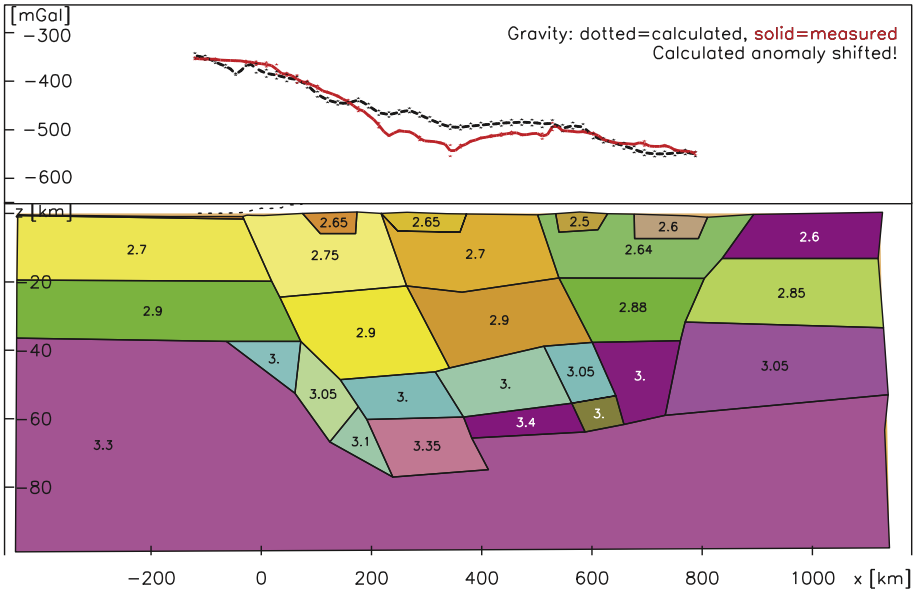

Fig. 12. Gravity modeling of an end-member model for the eclogitization of lower crust. The thick black line in upper part showing the computed gravity data, and the red line showing the measured gravity data. Filled points in lower part present the densities and velocities of 29 rock types atcanlibrated at room temperature and 600 MPa pressure. UC is upper crust, MC is middle crust and LC is lower crust, respectively. * Andesite (AND), Basalt (BAS), Diabase (DIA), Granite–granodiorite (GRA), Diorite (DIO), Gabbro–norite–troctolite (GAB), Metagraywacke (MGW), Slate (SLT), Phyllite (PHY), Prehnite–Pumpellyite Facies Basalt (BPP), Greenschist Facies Basalt (BGR), Granite-gneiss (GGN), Biolite (Tonalite) Gneiss (BGN), Mica Quartz Schist (QSC), Amphibolite (AMP), Felsic Granulite (FGR), Paragranulite (PGR), Anorthositic Granulite (AGR), Mafic Granulite (MGR), Serpentinite (SER), Quartzite (QTZ), Zeolite Facies Basalt (BZE), Mafic Garnet Granulite (GGR), Mafic-eclogite (ECL), Calcite Marble (MBL), Anorthosite (ANO), Hornblendite (HBL), Pyroxenite (PYX), Dunite (DUN).

The crustal structure of the Tibet plateau, in the area of latitude 26–34°N and longitude 82–92°E is investigated by three-dimensional gravity modeling constrained by deep seismic surveys. The calculated gravity field (Bouguer anomaly) of the initial density model (model I), which depends on the velocity structure linearly, misfits the observed data. By iterative changes in density and geometry of the interfaces (less than 2 km), the produced second density model (model II) matches better with the observed Bouguer anomaly data. Furthermore, since higher densities than global average densities are found in model II, lower-crustal partial eclogitization is considered in the final model (model III). Seven north–south trending density profiles are investigated by a 3-D gravity forward modeling method with geometry controlled by seismic data. The model implies large variations of the crustal structure from the western to the eastern part of central-south Tibet. The final model shows that dip angles of the Moho interface are near to 8.5° in the eastern and western part of the study area, which is smaller than the one found in the central part (~16.7°). We may infer that the Indian lithosphere underthrusts the Tibetan lithosphere gently in the eastern and western part of the central-south Tibet, while it is a little steeper in the central part, which indicates increased flexural rigidity of the lithosphere in the eastern and western part of the study area.

This study also provides a realistic crustal density structure as the basis for analyzing the petrologic properties in the crust of central-south Tibet. Integrating crustal P-wave velocity distribution from wide-angle seismic profiling, geothermal data and our crustal density model, we infer a crustal composition model, which is composed of an upper crust with granite–granodiorite and granite gneiss beneath the Lhasa block; biotite gneiss and phyllite beneath the Himalaya, a middle crust with granulite facies and possible pelitic gneisses, and a lower crust with gabbro–norite–troctolite and mafic granulite beneath the Lhasa block. Density values and composition in the lower crust indicates the absence of eclogite in the lower crust of central-south Tibet.

The presence of eclogite has been widely used in support of the theory of mass transfer from the lower crust to the underlying mantle by previous studies (Bousquet et al., 1997; Henry et al., 1997; Cattin et al., 2001; Tiwari et al., 2006; Hetenyi et al., 2007), and the presence of eclogite in the lower crust beneath the Lhasa block might also influence the topography of mountain ranges and plateaus in Tibet (Bousquet et al., 1997; Henry et al., 1997; Cattin et al., 2001), nevertheless our crust density values and composition structure in the lower crust do not support the existence of eclogite in the lower crust beneath central-south Tibet.

Acknowledgements

We are indebted to Professor Yong Wang of Institute of Geodesy and Geophysics, Chinese Academy of Sciences, he provided us the precious gravity data. We are grateful to the valuable help of Professor Giuliano. F. Panza and Doctor Fabio Romanelli in Trieste University in Italy. We would also like to thank Professor Zhongjie Zhang of IGGCAS (Institute of Geology and Geophysics, Chinese Academy of Sciences) for his constructive comments and suggestions that improved this paper. This study was financially supported by the National Basic Research Program of China (973 Program) (Grant Number 2011CB808904), the National Nature Science Foundation of China (Grant Numbers 41074033, 41021063), and the Ministry of the Land and Resources (Grant Number Sinoprobe-02-02).

References

Allègre, C.J., Courtillot, V., Tapponnier, P., Hirn, A., Mattauer, M., Coulon, C., Jaeger, J.J., Achache, J., Scharer, U., Marcoux, J., Burg, J.P., Girardeau, J., Armijo, R., Gariepy, C., Gopel, C., Li, T., Xiao, X., Chang, C., Li, G., Lin, B., Teng, J., Wang, N., Chen, G., Han, T., Wang, X., Den, W., Sheng, H., Cao, Y., Zhou, J., Qiu, H., Bao, P., Wang, S., Wang, B., Zhou, Y., Rong, H., 1984. Structure and evolution of the Himalaya–Tibet orogenic belt. Nature 307, 17–22.

Argand, E., 1924. La tectonique de l'Asie. In: 13th International Geological Congress. Brussels, pp. 170–372.

Bousquet, R., Goffé, B., Henry, P., Le Pichon, X., Chopin, C., 1997. Kinematic, thermal and petrological model of the Central Alps: lepontine metamorphism in the upper crust and eclogitisation of the lower crust. Tectonophysics 273, 105–127.

Braitenberg, C., Zadro, M., Fang, J., Wang, Y., Hsu, H.T., 2000. Gravity inversion in Qinghai-Tibet Plateau. Physics and Chemistry of the Earth, Part A: Solid Earth and Geodesy 25 (4), 381–386.

Braitenberg, C., Wang, Y., Fang, J., Hsu, H.T., 2003. Spatial variations of flexure parameters over the Tibet-Qinghai plateau. Earth and Planetary Science Letters 205, 211–224.

Brewer, I.D., Burbank, D.W., Hodges, K.V., 2003. Modelling detrital cooling-age populations: Insights from two Himalayan catchments. Basin Research 15, 305–320.

Breunig, M., Cremers, A.B., Götze, H.J., Schmidt, S., Seidemann, R., Shumilov, S., Siehl, A., 2000. Geologic mapping based on 3D models using an interoperable GIS. GIS-Journal for Spatial Information and Decision Making 13, 12–18.

Caen, H.L., Molnar, P., 1983. Constraints on the structure of the Himalaya from an analysis of gravity anomalies and a flexural model of the lithosphere. Journal of Geophysical Research 88 (B10), 8171–8191.

Cattin, R., Martelet, G., Henry, P., Avouac, J.P., Diament, M., Shakya, T.R., 2001. Gravity anomalies, crustal structure and thermo-mechanical support of the Himalaya of Central Nepal. Geophysical Journal International 147, 381–392.

Chatterjee, S., Goswami, A., Scoetese, C.R., 2012. The longest voyage: tectonic, magmatic and paleoclimatic evolution of the Indian plate during its northward flight from Gondwana to Asia. Gondwana Research. http://dx.doi.org/10.1016/j.gr.2012.07.001.

Chen, Y., Badal, J., Hu, J., 2009a. Love and Rayleigh wave tomography of the Qinghai-Tibet Plateau and surrounding areas. Pure and Applied Geophysics 167 (10), 1171–1203. http://dx.doi.org/10.1007/s00024-009-0040-1.

Chen, Y., Badal, J., Zhang, Z.J., 2009b. Radial anisotropy in the crust and upper mantle beneath the Qinghai-Tibet Plateau and surrounding regions. Journal of Asian Earth Sciences 36 (4–5), 289–302. http://dx.doi.org/10.1016/j.jseaes.2009.06.011.

Chen, Y., Zhang, Z., Sun, C., Badal, J., 2012. Crustal anisotropy from Moho converted Ps wave splitting analysis and geodynamic implications beneath the eastern margin of Tibet and surrounding regions. Gondwana Research. http://dx.doi.org/10.1016/j.gr.2012.04.003.

Christensen, N.I., Mooney, W.D., 1995. Seismic velocity structure and composition of the continental crust: a global view. Journal of Geophysical Research 100 (B7), 9761–9788.

Chung, S.L., Chua, M.F., Zhang, Y., Xie, Y., Lo, C., Lee, T.Y., Lan, C.Y., Li, X., Zhang, Q., Wang, Y., 2005. Tibetan tectonic evolution inferred from spatial and temporal variations in post-collisional magmatism. Earth-Science Reviews 68, 173–196.

Cotte, N., Pedersen, H., Campillo, M., Mars, J., Ni, J.F., Kind, R., Sandvol, E., Zhao, W., 1999. Determination of the crustal structure in southern Tibet by dispersion and amplitude analysis of Rayleigh waves. Geophysical Journal International 138, 809–819.

Dewey, J.F., Bird, J.M., 1970. Mountain belts and the new global tectonics. Journal of Geophysical Research 75, 2625.

Dewey, J.F., Burke, K.C.A., 1973. Tibetan, Variscan and Precambrian reactivation: products of continental collision. The Journal of Geology 81, 683–692.

Galve, A., Sapin, M., Hirn, A., Diaz, J., Lépine, J.C., Laigle, M., Gallart, J., Jiang, M., 2002. Complex images of Moho and variation of Vp/Vs across the Himalaya and South Tibet, from a joint receiver-function and wide-angle-reflection approach. Geophysical Research Letters 29 (2182). http://dx.doi.org/10.1029/2002GL015611.

Gao, R., Chen, X.Z., Wu, G.J., 1999. Lithospheric structure and geodynamic model of the Golmud-Ejn transect in northern Tibet. Geol. Soc. Am. 328, 9–17.

Götze, H.J., 1984. Uber den Einsatz interaktiver Computeraphik im Rahmen 3-dimensionaler Interpretationstechniken in Gravimetrie und Magnetik. Habil. Schrift, Technische Universitat Clausthal, ClausthalZellerfeld, Germany, 236 pp.

Götze, H.J., Lahmeyer, B., 1988. Application of three-dimensional interactive modeling in gravity and magnetic. Geophysics 53, 1096–1108.

Haines, S.S., Klemperer, S.L., Brown, L., Guo, J., Mechie, J., Meissner, R., Ross, A., Zhao, W., 2003. INDEPTH III seismic data: from surface observations to deep crustal processes in Tibet. Tectonics 22 (1001). http://dx.doi.org/10.1029/2001TC001305.

Harrison, T.M., Copeland, P., Kidd, W.S.F., Yin, A., 1992. Raising Tibet. Science 255, 1663–1670.

Hauck, M.L., Nelson, K.D., Brown, L.D., Zhao, W., Ross, A.R., 1998. Crustal structure of the Himalayan orogen at ~90 east longitude from Project INDEPTH deep reflection profiles. Tectonics 17, 481–500.

Henry, P., Le Pichon, X., Goffe, B., 1997. Kinematic, thermal and petrological model of the Himalayas: constraints related to metamorphism within the underthrust Indian crust and topographic elevation. Tectonophysics 273, 31–56.

Hetenyi, G., Cattin, R., Brunet, F., Bollinger, L., Vergne, J., Ńabelek, J.L.& Diament, M., 2007. Density distribution of the India plate beneath the Tibetan plateau: geophysical and petrological constraints on the kinetics of lower-crustal eclogitization. Earth planet Science Letters 264, 226-244, http://dx.doi.org/10.1016/j.epsl.2007.09.036.

Hirn, A., Jiang, M., Sapin, M., Diaz, J., Nercessian, A., Lu, Q.T., Lepine, J.C., Shi, D.N., Sachpazi, M., Pandey, M.R., MA, K., Gallart, J., 1995. Seismic anisotropy as an indicator of mantle flow beneaht the Himalayas and Tibet. Nature 375, 571–574.

Hirn, A., Nercessian, A., Sapin, M., Jobert, G., Xin, X.Z., Yuan, G.E., Jing, W.X., Yuan, L.D., Wen, T.J., 1984a. Lhasa block and bordering sutures—a continuation of a 500-km Moho traverse through Tibet. Nature 307, 25–27.

Hirn, A., Lepine, J.-C., Jobert, G., Sapin, M., Wittlinger, G., Xin, X.Z., Yuan, G.E., Jing, W.X., Wen, T.J., Bai, X.S., Pandey, M.R., Tater, J.M., 1984b. Crustal structure and variability of the Himalayan border of Tibet. Nature 307, 23–25.

Holmes, A., 1965. Principles of Physical Geology, second ed. Ronald Press, New York.

Hsu, H.T., Lu, Y., 1995. The regional geopotential model in China. Bollettino di Geodesia e Scienze Affiini LIV(N.2), 161–175.

Hu, J., Yang, H., Xu, X., Wen, L., Li, G., 2012. Lithospheric structure and crust-mantle decoupling in the southeast edge of the Tibetan Plateau. Gondwana Research 22, 1060–1067.

Jiang, M., Galve, A., Hirn, A., Voogd, B.de, Laigle, M., Su, H.P., Diaz, J., Lepine, J.C., Wang, Y.X., 2006. Crustal thickening and variations in architecture from the Qaidam Basin to the QangTang (North-Central Tibetan Plateau) from wide-angle reflection seismology. Tectonophysics 412, 121–140.

Jimenez-Munt, I., Fernandez, M., Jaume, V., John, P.P., 2008. Lithosphere structure underneath the Tibetan Plateau inferred from elevation, gravity and geoid anomalies. Earth and Planetary Science Letters 267, 276–289.

Jin, Y., McNutt, M.K., Zhu, Y.S., 1996. Mapping the descent of Indian and Eurasian plates beneath the Tibetan Plateau from gravity anomalies. Journal of Geophysical Research 101, 11275–11290.

Kaila, K.L., Narain, H., 1976. Evolution of the Himalaya based on seismo-tectonics and deep seismic soundings. In: Presented at the Himalaya Geology Seminar, Sponsor, Geological Survey of India, Delhi.

Kind, R., Ni, J., Zhao, W., Wu, J., Yuan, X., Zhao, L., Sandvol, E., Reese, C., Nabelek, J., Hearn, T., 1996. Evidence from earthquake data for a partially molten crustal layer in Southern Tibet. Science 274, 1692–1694.

Kumar, P., Yuan, X., Kind, R., Ni, J., 2006. Imaging the colliding Indian and Asian lithospheric plates beneath Tibet. Journal of Geophysical Research 111, B06308. http://dx.doi.org/10.1029/2005JB003930.

Le Fort, P., 1975. Himalaya: the collided range. Present knowledge of the continental arc. American Journal of Science 275A, 1–44.

Le Pichon, X., Henry, P., Goffé, B., 1997. Uplift of Tibet: from eclogites to granulites. Tectonophysics 273, 57–76.

Li, Q.S., 2003. The lithosphere structure of continental-continental collision in Tibet studied by seismology. PHD thesis.

Makovsky, Y., Klemperer, S., Huang, L., Lu, D.Y., 1996. Structural elements of the southern Tethyan Himalaya crust from wide-angle seismic data. Tectonics 15 (5), 997–1005.

McNamara, D.E., Walter, W.R., Owens, T.J., Ammon, C.J., 1997. Upper mantle velocity structure beneath the Tibetan Plateau from Pn travel time tomography. Journal of Geophysical Research 102, 493–505.

Meissner, R., Tilmann, F., Haines, S., 2004. About the lithospheric structure of central Tibet, based on seismic data from the INDEPTH III profile. Tectonophysics 380, 1–25.

Min, Z., Wu, F.T., 1987. Nature of the upper crust beneath central Tibet. Earth and Planetary Science Letters 84, 204–210.

Mengel, K., Kern, H., 1990. Petrologic versus seismic moho and crustal root mysteries. In: Freeman, R., Giese, P., Mueller, St., The European Geotraverse: Integrative Studies. Results From The Fifth Study Centre Rauischholzhausen (26 March-7 April 1990).

Minster, J.B., Jordan, T.H., 1978. Present-day plate motions. Journal of Geophysical Research 83 (B11), 5331–5354.

Mitra, S., Priestley, K., Bhattacharyya, A.K., Gaur, V.K., 2005. Crustal structure and earthquake focal depths beneath northeastern India and southern Tibet. Geophysical Journal International 160 (1), 227–248.

Molnar, P., 1988. A review of geophysical constraints on the deep structure of the Tibetan plateau, the Himalaya and the Karakoram, and their tectonic implications. Philosophical Transactions of the Royal Society of London A326, 33–88.

Molnar, P., Chen, W.P., Fitch, T.J., Tapponnier, P., Warsi, W.E.K., Wu, F.T., 1977. Structure and tectonics of the Himalaya: a brief summary of relevant geophysical observations. Himalaya: Sciences de la Terre, 269–294.

Nelson, K.D., Zhao, W., Brown, L.D., Kuo, J., Che, J.K., Liu, X.W., Klemperer, S.L., Makovsky, Y., Meissner, R., Mechie, J., Kind, R., Wenzel, F., Ni, J., Nabelek, J., Leshou, C., Tan, H.D., Wei, W.B., Jones, A.G., Booker, A., Unsworth, M., Kidd, W.S.F., Hauck, M., Alsdorf, D., Ross, A., Cogan, M., Wu, C.D., Sandvol, E., Edwards, M., 1996. Partially molten middle crust beneath southern Tibet: synthesis of project INDEPTH results. Science 274, 1684–1688.

Ni, J., Barazangi, M., 1984. Seismotectonics o f the Himalayan collision zone: geometry of the underthrusting Indian Plate beneath the Himalaya. Journal of Geophysical Research 89, 1147–1163.

Owens, T.J., Zandt, G., 1997. Implications of crustal property variations for models of Tibetan plateau evolution. Nature 387, 37–43.

Powell, C.M., Conaghan, P.J., 1973. Plate tectonics and the Himalayas. Earth and Planetary Science Letters 20 (1), 1–12.

Rajesh, R.S., Mishra, D.C., 2003. Admittance analysis and modelling of satellite gravity over Himalayas–Tibet and its seismogenic correlation. Current Science 84 (2), 224–230.

Schmidt, S., Götze, H.J., 1998. Interactive visualization and modification of 3D models using GIS functions. Physics and Chemistry of the Earth 23, 289–296.

Schulte-Pelkum, V., Monsalve, G., Sheehan, A., Pandey, M.R., Sapkota, S., Bilham, R., Wu, F., 2005. Imaging the Indian subcontinent beneath the Himalaya. Nature 435 (7046), 1222–1225.

Shin, Y.H., Xu, H., Braitenberg, C., Fang, J., Wang, Y., 2007. Moho undulations beneath Tibet from GRACE-integrated gravity data. Geophysical Journal International 170 (3), 971–985.

Sun, W., 1989. Bouguer Gravity Anomaly Map of the P.R. of China. Chinese Academy of Geoexploration, Beijing.

Teng, J., Wang, S.Z., Yao, Z.X., 1980a. Characteristic of the geophysical fields and plate tectonics of the Qinghai-Xizang Plateau and its neighboring regions. Acta Geophysica Sinica 23, 254.

Teng, J., Xiong S.B., Sun K.Z., 1980b. Explosion seismic study for velocity distribution and structure of the crust and upper mantle from Damzung to Yadong of Xizang Plateau. In: Proceedings of Symposium on Qinghai-Xizang Plateau (Abstracts), 81, Academia Sinica, Beijing.

Teng, J.W., Xiong, S.B., Yin, Z.X., 1985. Structure of the crust and upper mantle pattern and velocity distribution characteristics in the northern region of the Himalayan mountain region. Journal of Physical Earth 33, 157–171.

Tilmann, F., Ni, J., Team, I.I.S., 2003. Seismic imaging of the downwelling Indian lithosphere beneath central Tibet. Science 300 (5624), 1424–1427.

Tiwari, V.M., Vyghreswara Rao, M.B.S., Mishra, D.C., Singh, B., 2006. Crustal structure across Sikkim, NE Himalaya from new gravity and magnetic data. Earth and Planetary Science Letters 247, 61–69.

Unsworth, M., Wei, W., Jones, A.G., Li, S., Bedrosian, P.A., Booker, J.R., Jin, S., Deng, M., 2004. Crustal and upper mantle structure of northern Tibet imaged with magnetotelluric data. Journal of Geophysical Research 109, B02403. http://dx.doi.org/10.1029/2002JB002305.

Villasenor, A., Ritzwoller, M.H., Levshin, A.L., Barmin, M.P., Engdahl, E.R., Spakman, W., Trampert, J., 2001. Shear velocity structure of central Eurasia from inversion of surface wave velocities. Physics of the Earth and Planetary Interiors 123, 169–184.

Wang, Y., Zheng, J., Zheng, J., Zhang, W., Li, S., Liu, X., Yang, X., Liu, Y., 2012. Cenozoic uplift of the Tibetan Plateau: evidence from the tectonic-sedimentary evolution of the western Qaidam Basin. Geoscience Frontiers 3, 175–187.

Wei, W., Unsworth, M., Jones, A., Booker, J.R., Tan, H., Nelson, K.D., Chen, L., Li, S., Solon, K., Bedrosian, P.A., Jin, S., Deng, M., Ledo, J., Kay, D., Roberts, B., 2001. Detection of widespread fluids in the Tibetan crust by magnetotelluric studies. Science 292, 716–718.

Wu, G.J., Xiao, X.C., Li, T.D., 1993. Lithospheric structure and evolution of the Tibetan Plateau: theYadong–Golmud Geoscience transect. Tectonophysics 219, 213–221.

Xia, L., Li, X., Ma, Z., Xu, X., Xia, Z., 2011. Cenozoic volcanism and tectonic evolution of the Tibetan plateau. Gondwana Research 19, 850–866.

Xiong, S.B., Liu, H.B., 1997. Crustal structure in the west Tibetan plateau. Chinese Science Bulletin 42 (12), 1309–1312 (in Chinese).

Xiong, S.B., Teng, J.W., Yin, Z.X., 1985. The thickness of the crust and undulation of discontinuity in Xizang (Tibet) plateau. Chinese Journal of Geophysics (Acta Geophysica Sinica) 28, 16–27 (in Chinese).

Yuan, X., Ni, J., Kind, R., Mechie, J., Sandvol, E., 1997. Lithospheric and upper mantle structure of southern Tibet from a seismological passive source experiment. Journal of Geophysical Research 102, 27491.

Zhang, Z.J., Klemperer, S.L., 2005. West–east variation in crustal thickness in northern Lhasa block, central Tibet, from deep seismic sounding data. Journal of Geophysical Research 110 (B9), B09403. http://dx.doi.org/10.1029/2004JB003139.

Zhang, Z.J., Klemperer, S., 2010. Crustal structure of the Tethyan Himalaya, southern Tibet: new constraints from old wide-angle seismic data. Geophysical Journal International 181 (3), 1247–1260.

Zhang, Z.J., Li, Y., Wang, G., Teng, J., Klemperer, S., Li, J., Fang, J., Chen, Y., 2002. East–west crustal structure and "down-bowing" Moho under Northern Tibet as revealed by wide-angle seismic profile. Science in China, Series D: Earth Sciences 45, 550–558.

Zhang, Z.J., Zhang, X., Badal, J., 2008. Composition of the crust beneath southeastern China derived from an integrated geophysical data set. Journal of Geophysical Research 113 (B4), B04417. http://dx.doi.org/10.1029/2006JB004503.

Zhang, X., Louisa, L.H., Wang, Y., Zhao, B., 2009a. Petrologic composition model of the upper crust in Bohai Bay basin, China, based on Lamé impedances. Applied Geophysics 6, 327–336.

Zhang, Z.J., Wang, Y.H., Chen, Y., Houseman, G.A., Tian, X.B., Wang, E.R., Teng, J.W., 2009b. Crustal structure across Longmenshan fault belt from passive source seismic profiling. Geophysical Research Letters 36, L17310. http://dx.doi.org/10.1029/2009GL039580.

Zhang, Z.J., Yuan, X.H., Chen, Y., Tian, X.B., Kind, R., Li, X.Q., Teng, J.W., 2010. Seismic signature of the collision between the east Tibetan escape flow and the Sichuan Basin. Earth and Planetary Science Letters 292 (3–4), 254–264.

Zhang, Z.J., Deng, Y.F., Teng, J.W., Wang, C.Y., Gao, R., Chen, Y., Fan, W.M., 2011a. An overview of the crustal structure of the Tibetan plateau after 35 years of deep seismic soundings. Journal of Asian Earth Sciences 40 (4), 977–989.

Zhang, Z.J., Klemperer, S., Bai, Z.M., Chen, Y., Teng, J.W., 2011b. Crustal structure of the Paleozoic Kunlun orogeny from an active-source seismic profile between Moba and Guide in East Tibet, China. Gondwana Research 19 (4), 994–1007.

Zhang, Z., Yang, L., Teng, J., Badal, J., 2011c. An overview of the earth crust under China. Earth-Science Reviews 104, 143–166. http://dx.doi.org/10.1016/j.earscirev.2010.10.003.

Zhang, Z.M., Dong, X., Santosh, M., Zhao, G.C., 2012. Metamorphism and tectonic evolution of the Lhasa terrane, Central Tibet. Gondwana Research, http://dx.doi.org/10.1016/j.gr.2012.08.024.

Zhao, L.S., Sen, M., Stoffa, P., Frohlich, C., 1996. Application of very fast simulated annealing to the determination of the crustal structure beneath Tibet. Geophysical Journal International 125, 355–370.

Zhao, W.J., Neilson, K.D., Project INDEPTH Team, 1993. Deep seismic reflection evidence for crustal underthrusting beneath southern Tibet. Nature 366, 557–559.

Zhao, W.J., Mechie, J., Brown, L.D., Guo, J., Haines, S., Hearn, T., Klemperer, S.L., Ma, Y.S., Meissner, R., Nelson, K.D., Ni, J.F., Pananont, P., Rapine, R., Ross, A., Saul, J., 2001. Crustal structure of central Tibet as derived from INDEPTH wide angle seismic data. Geophysical Journal International 145, 486–498.

Zhao, B., Bai, Z., Xu, T., Badal, J., 2012. Composition of the South China crust based on integrated geophysical data. Journal of Geophysics and Engineering, submitted for publication.

Zhao, J.M., Mooney, W.D., Zhang, X.K., Li, Z.C., Jin, Z.J., Okaya, N., 2006. Crustal structure across the Altyn Tagh Range at the northern margin of the Tibetan plateau and tectonic implications. Earth and Planetary Science Letters 241, 804–814.

Zheng, D., Yao, T.D., 2004. Uplift of Tibetan plateau with its environmental effects. Science Press, Beijing, pp. 60–65 (in Chinese).